NASA Electronic Parts and Packaging (NEPP) Program

NEPP Task:

Reliability Effects of Surge Current Testing of Solid Tantalum Capacitors

Alexander Teverovsky

Perot Systems,
Code 562, NASA GSFC, Greenbelt, MD 20771

Alexander.A.Teverovsky.1@gsfc.nasa.gov

December 2007

I. Introduction.

Solid tantalum capacitors are widely used in space applications to filter low-frequency ripple currents in power supply circuits and stabilize DC voltages in the system. Tantalum capacitors manufactured per military specifications (MIL-PRF-55365) are established reliability components and have less than 0.001% of failures per 1000 hours (the failure rate is less than 10 FIT) for grades D or S, thus positioning these parts among electronic components with the highest reliability characteristics.

Still, failures of tantalum capacitors do happen and when it occurs it might have catastrophic consequences for the system. This is due to a short-circuit failure mode, which might be damaging to a power supply, and also to the capability of tantalum capacitors with manganese cathodes to self-ignite when a failure occurs in low-impedance applications. During such a failure, a substantial amount of energy is released by exothermic reaction of the tantalum pellet with oxygen generated by the overheated manganese oxide cathode, resulting not only in destruction of the part, but also in damage of the board and surrounding components.

A specific feature of tantalum capacitors, compared to ceramic parts, is a relatively large value of capacitance, which in contemporary low-size chip capacitors reaches dozens and hundreds of microfarads. This might result in so-called surge current or turn-on failures in the parts when the board is first powered up. Such a failure, which is considered as the most prevalent type of failures in tantalum capacitors [1], is due to fast changes of the voltage in the circuit, dV/dt, producing high surge current spikes, $I_{sp} = C \times dV/dt$, when current in the circuit is unrestricted. These spikes can reach hundreds of amperes and cause catastrophic failures in the system. The mechanism of surge current failures has not been understood completely yet, and different hypotheses were discussed in relevant literature. These include a sustained scintillation breakdown model [1-3]; electrical oscillations in circuits with a relatively high inductance [4-6]; local overheating of the cathode [5, 7, 8]; mechanical damage to tantalum pentoxide dielectric caused by the impact of MnO_2 crystals [2, 9, 10]; or stress-induced-generation of electron traps caused by electromagnetic forces developed during current spikes [11].

A commonly accepted explanation of the surge current failures is that at unlimited current supply during surge current conditions, the self-healing mechanism in tantalum capacitors does not work, and what would be a minor scintillation spike if the current were limited, becomes a catastrophic failure of the part [1, 12]. However, our data show that the scintillation breakdown voltages are significantly greater that the surge current breakdown voltages, so it is still not clear why the part, which has no scintillations, would fail at the same voltage during surge current testing (SCT).

A risk of using of an electronic component, and a tantalum capacitor in particular, can be defined as a product of the probability of failure and consequences (expressed for example as the cost of rework, retesting, redesign, project delays, etc.). In this regard, tantalum capacitors can be considered as low failure rate parts with a high risk of application. To reduce this risk, further development of a screening and qualification system with special attention to the possible deficiencies in the existing procedures is necessary.

The existing system of screening and qualification of tantalum capacitors per MIL-PRF-55365 is supposed to assure that the parts would operate reliably at two operating environments: steady-state and surge current conditions. A so-called Weibull grading test, which is a version of a burn-in performed typically at 85 ^{o}C and voltages varying from 1.1VR to 1.53VR for at least 40 hours, is used to assure that failure rate of the parts at steady-state conditions is below the required level. Surge current testing is used to eliminate possible failures in applications under surge current conditions.

Surge current testing became a standard for high-reliability applications and is mandatory for application of tantalum capacitors for all levels of space systems (NASA/GSFC EEE-INST-002). During SCT, a part is stressed 10 times with high current spikes produced by discharging of a large capacitor charged to the rated voltage, VR, onto the part under test. It is important to mention that typically during screening the parts are stressed at conditions above rated to separate and/or burn out potentially weak parts. The Weibull grading and voltage surge tests per MIL-PRF-55365 are examples of screens performed at stress voltages substantially exceeding the rated ones. However, surge current testing is required to be carried out at the rated voltages only. This does not assure necessary quality margins in the product, and places the burden of providing reliability of the component on customers, forcing them to substantially (up to 70% in some cases) derate application voltages.

In spite of the obvious importance of SCT, this test is still optional per MIL-PRF-55365. More than that, even its position in the manufacturing process, in particular, whether to perform it before (option C) or after (option B) Weibull grading or voltage ageing tests, is left to customer choice. Some customers believe that SCT might damage the tantalum pentoxide dielectric, and hence this test should be carried out before the Weibull grading with the hope that the parts degraded by SCT would be screened out by burning in. One might also speculate that the long-term high-voltage stress at high temperatures might degrade the capability of capacitors to withstand surge current stresses, and thus the SCT should be carried out after Weibull grading. Unfortunately, neither of the opinions has been substantiated by adequate engineering analysis, and decisions are often made based on unverified data. The situation with the surge current screening is likely a reflection of uncertainty about the mechanism of failure and processes causing possible degradation of the parts. Also, there is only scarce experimental data on the effect of surge current events on the reliability of tantalum capacitors.

An attempt to evaluate the effect of the surge current testing on long-term reliability of the parts was performed by Sprague Electric under NASA contract NAS8-33424 more that 30 years ago [13]. However, the results were inconclusive due to a small number of failures. More recently [7], life testing of the capacitors after multiple, 10000 surge cycles at the rated voltage was performed and showed no detectable difference in results as compared to the reference samples.

Experience shows that parts that have passed SCT screening during manufacturing might fail during applications or when a surge current test is repeated by a user. There might be several reasons for this to happen:

1. Non-adequate test conditions resulting in different level of stress in different test set-ups used in different laboratories.

2. Environmentally-induced stresses and/or soldering might cause degradation and reduction of the surge current breakdown voltage.
3. Screening with 10 cycles does not guarantee that the part will not fail during cycle 11 and higher.
4. During manufacturing, SCT is typically performed on capacitors connected to the lead frame, so it is possible that mechanical stresses during cutting and forming the leads create defects reducing surge current breakdown voltages.
5. There is always a possibility that a defective part escapes the screening due to operator mistakes or equipment problems.

The latter of the reasons should be resolved on the management level, but the rest require engineering analysis and experimental verifications.

SCT test conditions have been analyzed in our previous work [14] where the possibility of substantial variations of the test results even when formal requirements of MIL-PRF-55365 are satisfied has been demonstrated. It has been shown in [15] that variations in the resistance of the SCT circuit, even in the range allowed per MIL-PRF-55365, exponentially change breakdown voltages during the testing. Analysis of additional factors affecting results of SCT will be considered in section II of this report.

Environmental stress testing and, in particular, temperature cycling and exposure to high temperatures, can damage the parts and potentially create surge current failures [16]. Soldering is considered as one of the major factors contributing to the first turn-on failures and proofing or controlled power-up of the parts [17] has been suggested to reduce the probability of soldering-induced failures. Some manufacturers have employed this technique to improve reliability of DC-DC converters by initiating the self-healing mechanism in the output tantalum capacitors, which might have been damaged after soldering. However, more data are necessary to understand the relationship between environmental factors and surge current failures, and to develop a better qualification system allow identification and rejection of lots with poor resistance to environmental stresses.

Failures during SCT are typically accompanied by substantial acoustic, mechanical, and thermal effects. This allows the assumption that even parts that have passed SCT screening might have experienced stresses sufficient to degrade their characteristics and compromise reliability. Although characteristics of the parts are required to remain within the specified limits after the test, it is conceivable that some degradation still occurs. This is due to the fact that typically the specified range of characteristics is too wide to observe possible degradation. For example, requirements for leakage currents are normally two to three orders of magnitude greater than real leakage currents. In this case, even parts with significantly increased DCL after SCT would be considered as normal, and no degradation would be detected.

Most researchers agree that SCT screening does not affect characteristics and quality of the parts. Experiments showed that even 1 million surge current cycles with spikes of 12 A to 40 A did not shift capacitance, ESR, or leakage current of the tested parts [18]. It is commonly accepted that failures during SCT screening happen mostly after the first few surge cycles [13], and this apparently justifies the choice of 10 cycles for screening at rated voltages. Franklin [4] noted that

failures at several cycles are more likely to occur during testing at voltages higher than the rated. However, no detailed analysis of the possibility of surge current failures at increased numbers of cycles has been discussed so far, and the probability of post-screening surge current failures has not been estimated. If such a possibility is real, then the screening procedure and the methodology of analysis of factors affecting the capability of the parts to withstand surge current conditions might need to change. Otherwise, SCT failures observed after certain stress testing on parts that have passed the screening, might create a false impression that these stresses have degraded the capability of parts to withstand surge current conditions. This might result in erroneous conclusions regarding the quality of the parts and/or the effectiveness of the screening and qualification procedures used.

The purpose of this work is evaluation of the effect of surge current stress testing on characteristics and reliability of tantalum capacitors at both long-term steady-state and multiple surge current stress conditions. In order to reveal possible degradation and precipitate more failures, various part types were tested and stressed in the range of voltage and temperature conditions exceeding the specified limits. A model to estimate the probability of post-SCT-screening failures and measures to improve the effectiveness of the screening process has been suggested.

Content.

II. Experiment.

II.1 Parts.

Ten different types of commercial tantalum capacitors have been used in this study. Table II.1 shows the part types used and their specified characteristics, including capacitance (C), rated voltage (VR), effective series resistance (ESR), DC leakage current (DCL), and dissipation factor (DF). Most of the parts were remnants from the lots used in various GSFC projects, so they represent capacitors typically used in space applications. The part types selected for this study had high CV values varying from 525 μF-V to 3300 μF-V and had a relatively large size of 7343 per EIA size code.

Table II.1. Solid tantalum capacitors used in this study.

PN	Mfr	C, μF	VR, V	DC	ESR, mOhm	DCL at RT, μA	DF, %
T495X336K035AS	KEMET	33	35	0128YE30		11.6	6
T495X107K016AS	KEMET	100	16	0052K750		16	8
T510X337K010AS	KEMET	330	10	0038H540		33	10
T495X476K020ASE150	KEMET	47	20	0429R	150	7.5	4
T495X227K006ASE100	KEMET	220	6	0532	100	13.2	8
TPSD476K020R0100	AVX	47	20	(2006)	100	9.4	6
TPSD336K035R0200	AVX	33	35	(2006)	200	11.6	6
T495156M035AHE225	KEMET	15	35	0542	225	5.3	6
T495X156M050AS	KEMET	15	50	0405		7.5	8
T491D226M035AS	KEMET	22	35	0408		7.7	6

VIII.4 Surge current testing.

A test setup used for surge current testing (SCT) is shown in Figure II.1. Note that this setup is in compliance with MIL-PRF-55365; however, to increase the amplitude of surge current spike, no limiting resistors were used (up to 1.2 Ohm is allowed per MIL-PRF-55365). Four power MOSFETs, IRL2910S, manufactured by International Rectifier, were connected in parallel and used to discharge the bank capacitor (CB) onto the device under test (DUT). Each of the transistors was capable of withstanding current spikes up to 190 A and had a rated resistance of 26 mOhm at 55 A. The bank capacitor had a value of 13,600 μF and was comprised of two aluminum electrolytic SMH 6800 μF/100 V capacitors manufactured by Nippon Chemi-Con. A film power 100 Ohm resistor, RPS, was used between the power supply and CB to limit inrush currents in the bank capacitor during charging.

Oscillograms of the charge current spikes were monitored using a Tektronics AM503 current probe amplifier and a digital oscilloscope, Infinium, manufactured by Hewlett Packard. A precision semiconductor analyzer, hp4156A, was used to provide and monitor current to charge CB, generate gate pulses to open the switch, and record the amplitudes of current spikes, applied

voltages, and currents, Ic, at the end of the charging cycle. Switching pulses were applied after 9.9 seconds of charging of the bank capacitor for 100 milliseconds as shown in the timing diagram in Figure II.1b. Following the surge event, the system was discharged for 6 seconds, after which the test could be repeated. The program allowed for setting the number of surge cycles, Nc, initial test voltage, V_o, and voltage increments between the steps, ΔV, to carry out step stress surge current testing (3SCT), which typically begins with the rated voltage and continues until a failure occur. By setting V_o = VR, N_c = 10, and ΔV = 0, a test per MIL-PRF-55365 could be carried out.

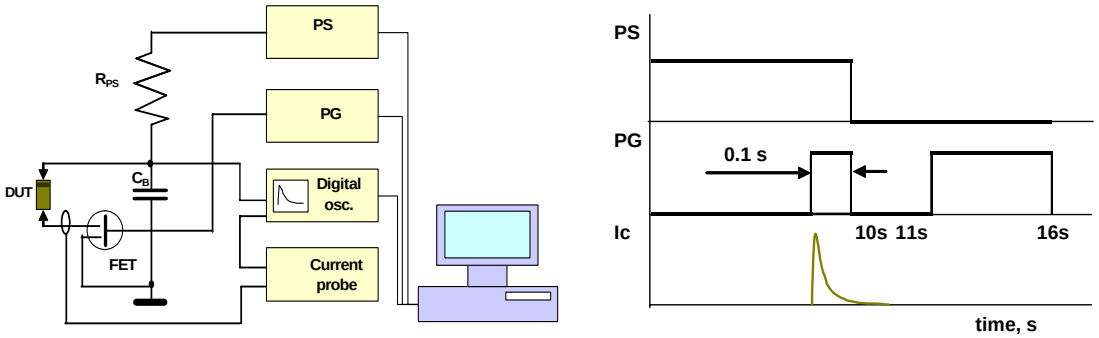

a) b)

Figure II.1. Test setup (a) and timing diagram (b) of the surge charge current testing.

An example of oscillograms observed during 3SCT of 47μF/20V capacitors is shown in Figure II.2a and Figure II.2b shows failure events of 15μF/50V capacitors. The failure could be clearly observed by increased currents after the transient completion, typically after 20 to 50 μs for different part types. For this reason the program acquired the current after 80 μs, I_{80}, and if I_{80} was greater than 2 A, a breakdown was recorded and the program stopped. Another failure condition used to obtain reliable detection of the breakdown event automatically, was charge current after 10 seconds of charging, I_{10}. An increase of I_{10} (caused by increased leakage current of DUT after breakdown) to more than 10 mA indicated a failure, also stopped the program, and recorded the data.

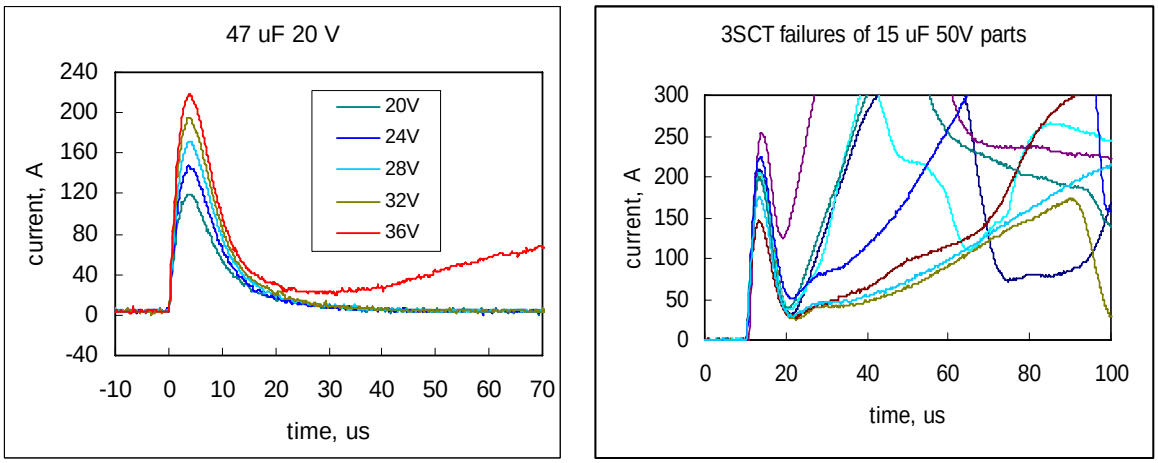

a) b)

Figure II.2. Typical current spikes during step stress surge current testing for 47 μF 20 V capacitors (a), and SCT failures at voltages varying from 60 V to 100 V in 15 μF 50 V parts (b).

Note that the high-current spikes observed during the first 20 to 50 microseconds of SCT are displacement currents flowing through the tantalum pentoxide dielectric, while currents indicating a failure event (typically within 0.1 to 1 ms after the surge) are due to conduction in the damaged dielectric. When a failure occurs, a substantial amount of heat is dissipated in the tested capacitor often resulting in a dramatic acoustic effect (explosion), mechanical fracture of the package, and smoke generated by overheated/burnt molding compound. In some cases, the part can catch fire as shown in Figure II.3 (this is more likely to happen for high-value capacitors). For this reason, special safety measures have to be taken to reduce hazards related to smoke generation and fire in the setup.

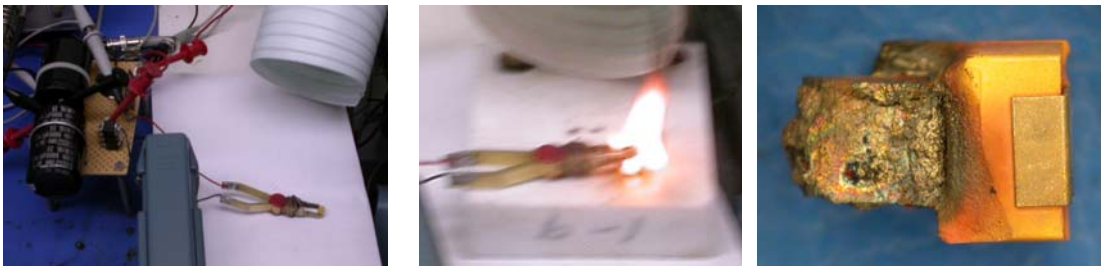

a) b) c)

Figure II.3. A setup with a clamp for DUT and an air cleaning system used during SCT (a), a 330 µF/10 V capacitor catching fire during testing at 10 V (b), and a view of a burnt-out capacitor after the test (c).

Figure II.4a shows typical oscillograms observed during 3SCT of 220µF/6V capacitors. Based on these data, the amplitudes of current spikes, I_{sp}, were plotted against the applied voltage for several part types as shown in Figure II.4b. The results clearly indicate a linear relationship between I_{sp} and V, thus allowing calculation of the effective resistance, R_{eff}, of the surge current test circuit.

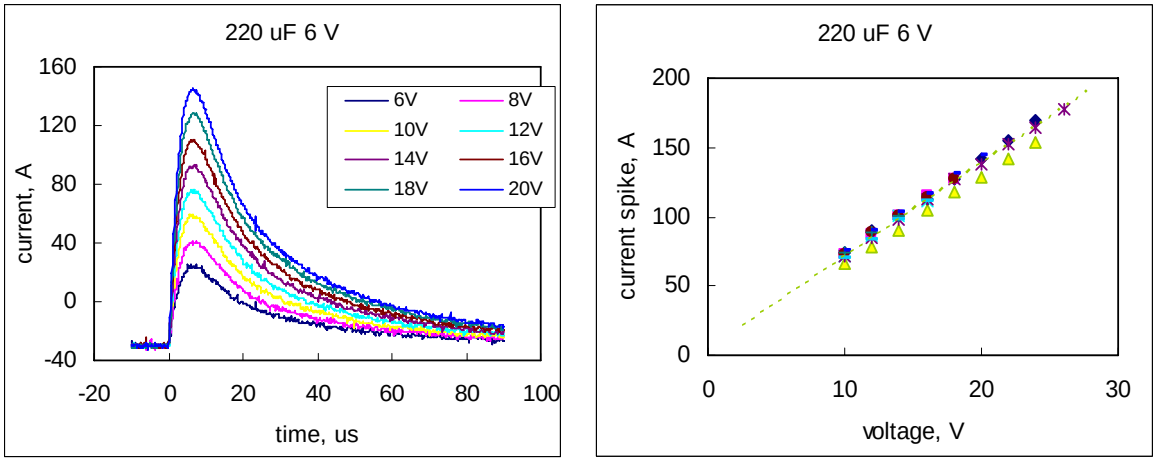

a) b)

Figure II.4. Current spikes in a 220 µF 6 V capacitor (a), and variation of the amplitude with voltage for nine samples (b). The slope of the lines indicates the effective resistance, R_{eff}, which in this case had an average value of 149 milliohms and a standard deviation of 4 milliohms.

The value of R_{eff} was found to correlate with the ESR values of the tested capacitors as can be seen in Figure II.5. This indicates that the used setup does not introduce substantial additional impedance (active, caused by contacts and wires, or inductive, caused by the length of interconnections) to the circuit, and that the ESR value is a major contributor to the resistance of the circuit. The value of R_{eff} is important to characterize the setup used and is an effective means to assure proper, low-resistive contacts to the DUT and adequate operation of the SCT circuit.

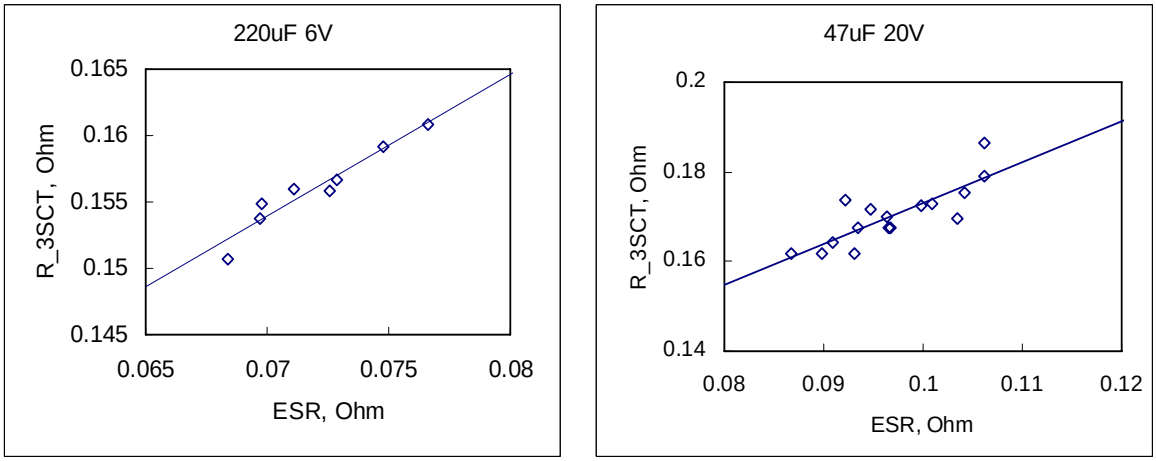

a) b)

Figure II.5. Correlation between ESR and the effective resistance, R_{eff}, of the SCT calculated as a slope of Isp vs. V relationship for 220 µF 6 V (a) and 47 µF 20 V (b) capacitors.

To assure reproducibility of results during SCT, it is important that the characteristics of the switch are not degrading after application of multiple high-current pulses. To verify the stability of the FETs used, characteristics of the transistors were measured periodically after multiple 100 A pulses were applied during testing of 50 V capacitors. Results of these measurements are shown in Figure II.6, indicating high reproducibility of the characteristics. No degradation of the parts occurred even after 22 million current spikes had been applied.

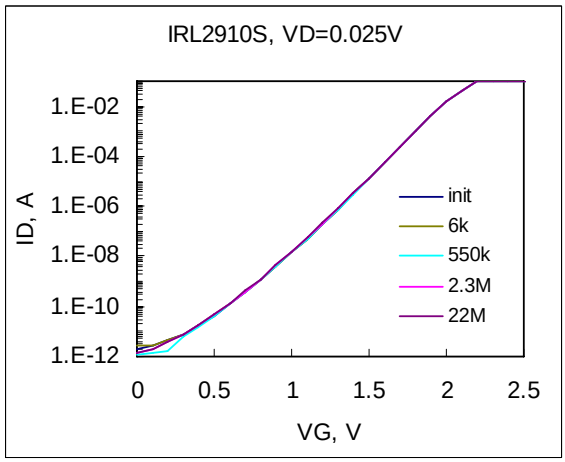

Figure II.6. Transfer characteristics of the power FET (PN IRL2910S) used as a switch in the set-up shown in Figure II.1. The characteristics were measured periodically after SCT testing at

average current pulses of more than 100 A up to 22 million cycles and indicate no degradation of the FET. The resistance of the switch remained within the 65-66 mOhm range.

VIII.5 Surge current discharge testing.

A setup for the current discharge test (see Figure II.7) was similar to the one described above. The DUT was charged through a 100-Ohm resistor, R_{PS}, for 9.9 seconds at a set voltage by a power supply. After charging, a 100-millisecond pulse opened the FET, causing a discharge current spike from the capacitor to flow through the FET.

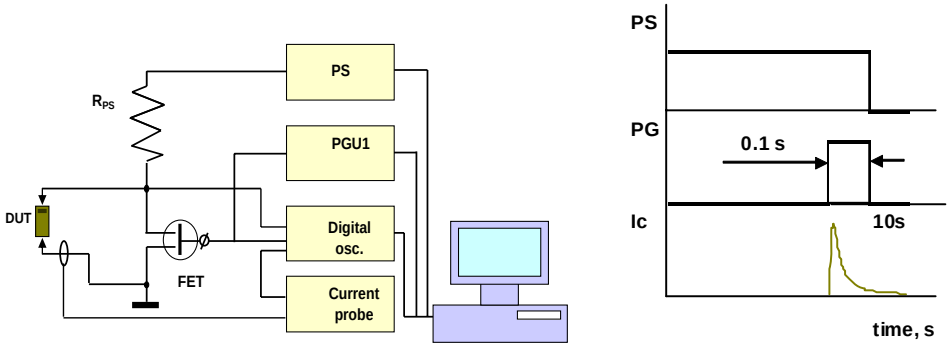

a) b)

Figure II.7. Test setup (a) and timing diagram (b) of the surge discharge current test.

Typical oscillograms of the step stress discharge current testing of a 15 µF/50 V capacitor at voltages varying from 10 V to 100 V are shown in Figure II.8a. Figure II.8.b shows that variations of the current spike amplitudes with applied voltage for the charge and discharge conditions are similar, indicating that circuits with similar external resistances were used.

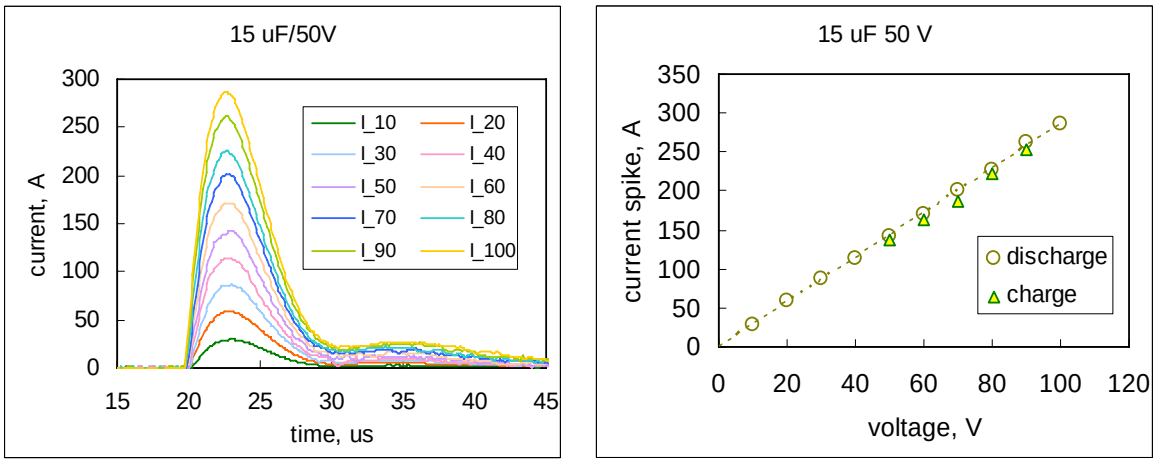

a) b)

Figure II.8. Current oscillograms during step stress discharge current test of a 15 µF 50 V capacitor in the range from 10 to 100 V (a), and variations of current spike amplitudes with voltage for the step stress charge and discharge tests (b).

Similar to 3SCT, step stress discharge current testing resulted in reproducible $I_{sp}(V)$ characteristics as shown in Figure II.9. The calculated R_{eff} values averaged to 246 mOhm and standard deviation of 4.2 mOhm. Similar to 3SCT, the values of R_{eff} correlated with ESR of the parts. No failures were observed up to stress voltage of 89 V, which means that VBR > 89 V. Note that the average breakdown voltage during 3SCT for these parts was much less, VBR_3SCT = 72 V at STD = 5.8. This indicates that the current spike is not a major cause of the surge current-induced breakdown, and the presence of voltage after spike is completed is necessary to cause failure.

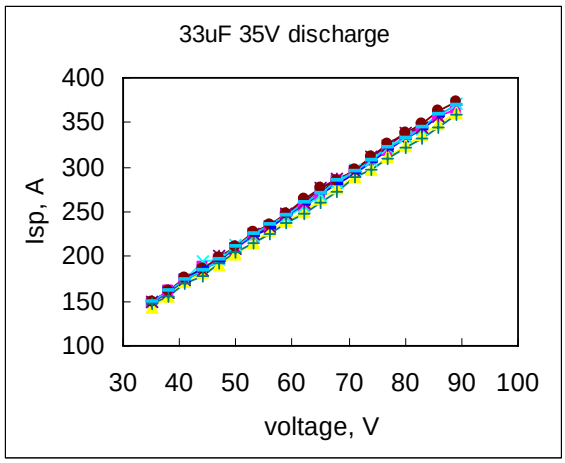

Figure II.9. Variations of current spike amplitudes with voltage during 3SCT discharge test for nine samples of 33 μF 35 V capacitors.

VIII.6 Effect of test conditions on results of SCT.

VIII.6.1 Length of wires.

Our previous analysis [14] showed that the length of wires, used to connect the DUT to the bank capacitor and the switch, increase inductance in the circuit and can reduce the amplitude of current spikes. In this study, experiments with different lengths of wires were carried out during SCT of 47 μF/20 V and 220 μF/6 V capacitors. Typical results of the test are shown in Figure II.10 and indicate approximately 1.7 times decrease of Isp from 130A for 4" wires to 75 A for 24" wires. This is close to the changes expected from the calculations (~1.65 times).

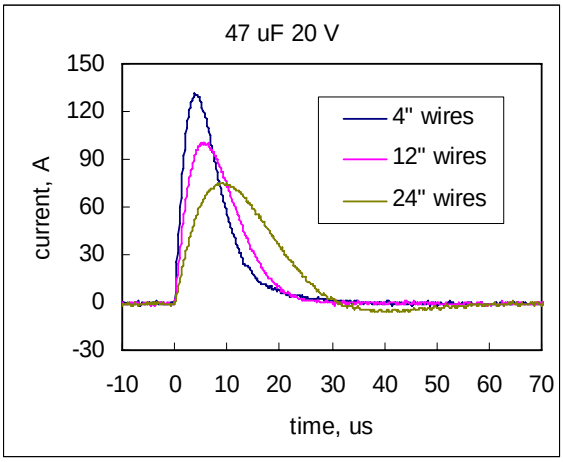

Figure II.10. Effect of the wire length (22 AGW) between the test setup output and DUT for 47 μF 20 V capacitors tested at 20 V.

Statistical data obtained during 3SCT of the parts in a setup with long wires used for testing in a temperature chamber (10" wires) and short, 3", wires used during regular SCT at room temperature are displayed in Table II.2. The results show a significant decrease in the average R_{eff} as the length of wires decreases from 10" to 3", 1.65 times for 47 μF/20 V capacitors and 1.57 times for 220 μF/6 V capacitors. However, the breakdown voltages only slightly, ~5 %, increased with the wire length for 47 μF/20 V parts and did not change significantly for 220 μF/6 V parts. This is consistent with the results of previous study [4], suggesting that voltage might be more important than current in initiating the surge failures.

Table II.2. Effect of the wire length on the effective resistance and breakdown voltage during 3SCT of 47uF/20V and 220uF/6V capacitors.

Capacitor	Wires	QTY	VBR_3SCT		Effecive resistance	
			VBR_avr	STD	Reff, mOhm	STD
47uF/20V	10" wires	15	46	7.23	266	9.9
	3" wires	15	43.67	7.69	161	7.3
220uF/6V	10" wires	10	20.4	3.5	173	3.5
	3" wires	27	21.7	4.2	110	6.2

One of the reasons of a relatively weak dependence of the VBR_3SCT on the length of the wires might be related to the fact that inductance of the circuit reduces the amplitude of the spike, but increases its width, so the energy dissipated in the part is not changing. However, more data are necessary to evaluate the effect of circuit inductance on the surge current breakdown voltages.

VIII.6.2 FET switching pulse.

Another factor that was found affecting the amplitude of the current spike is the shape of the switching pulse applied to the gate of the FET used to initiate the discharge in the circuit. The input capacitance of the FETs used is rather large, C = 14800 pF, so application of ~ 1 kOhm

resistor, R_G, between the pulse generator and the gate would cause the gate voltage to increase exponentially with a time constant, RC, of ~ 15 μs. This condition would slightly slow the opening of the switch, thus allowing bleeding of the current from DUT in the process of switching and reducing the amplitude of current spikes. Results of SCT experiments carried out with 47 μF/20 V capacitors and R_G of 0.8 kOhm and 1.6 kOhm (the corresponding RC values are 11.8 μs and 23.7 μs) are shown in Figure II.11 and indicate a significant decrease in the spike currents. This means that use of high-value limiting resistors should be avoided, and special care should be taken to assure abrupt gate pulses. Note also, that the reduction of current spike amplitude caused by the shape of the gate pulse might change the amount of energy dissipated in the part and thus affect the results of SCT.

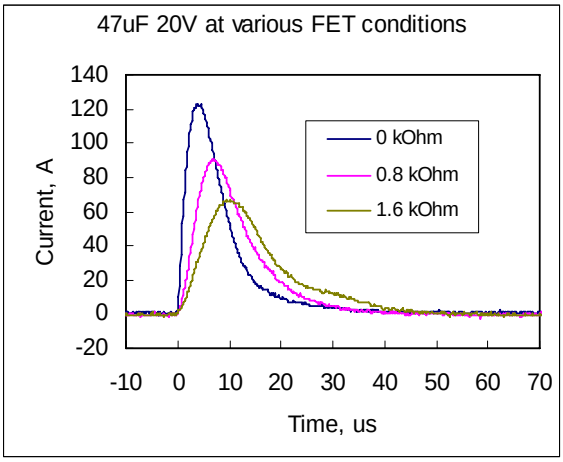

Figure II.11. Effect of resistance between the pulse generator and gate of the FET on current spike oscillograms during testing of 47 μF 20 V capacitors at 20 V.

VIII.6.3 Temperature.

MIL-PRF-55365 allows optional testing of the parts at -55 °C and +85 °C or at room temperature only (it is not clear why a three-temperature test is not recommended). Unfortunately, only limited data are available on the effect of temperature on the surge current breakdown voltages. It has been shown that temperature substantially increases the proportion of failures from 7% at RT to 60% at 85 °C and to 80% at 125 °C for 25 V rated capacitors tested at 40 V [4]. Moynihan [13] suggested an exponential dependence of turn-on failures with temperature and estimated the activation energy of 0.55 eV.

To evaluate the effect of temperature on results of 3SCT, three types of capacitors (15 μF/50V, 47 μF/20V, and 220 μF/6V) with 9 to 15parts each group were tested in a temperature chamber. Two part types were tested at temperatures suggested by MIL-PRF-55365 and one part type was tested at a wider range of temperatures, from liquid nitrogen (-196 °C) to +125 °C. Statistical data presenting results of these tests are shown in Table II.3 and Figures II.12 to II.14.

Table II.3. Effect of temperature on effective resistances and breakdown voltages during surge current testing.

Capacitor	T, °C	QTY	VBR_3SCT		Effecive resistance	
			VBR_avr	STD	R_{eff}, mOhm	STD
15 µF/50V	-196	10	73	6.7	760	19
	-55	12	78.3	9.4	470	21
	+20	11	82.4	11.6	405	8.5
	+125	10	72	11.4	320	12
47 µF/20V	-55	10	53.6	6.5	245	22
	+20	15	46	7.2	335	17
	+85	13	38.2	5.8	265	10
220 µF/6V	-55	9	23.5	2.2	215	10
	+20	10	20.4	3.5	175	3.5
	+85	13	18.6	4.5	168	10

In all cases the data suggest a significant decrease of R_{eff} with temperature, which is most likely due to a decrease in ESR values. It is known that ESR depends on the resistivity of the manganese cathode layer, which is a semiconductor with a relatively shallow donor level of ~ 0.04 eV [19]. Our data indicated exponential variations of R_{eff} with Ea in the range from 0.012 to 0.015 eV, which is consistent with the literature data for MnO_2.

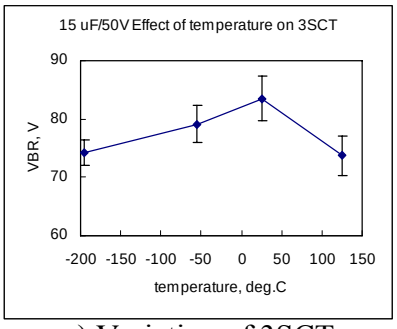

a) Variation of 3SCT breakdown voltages with temperature

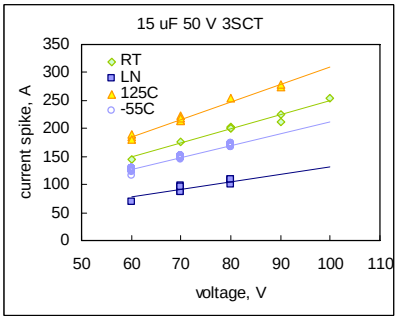

b) Variations of current spike amplitudes with voltage at different temperatures

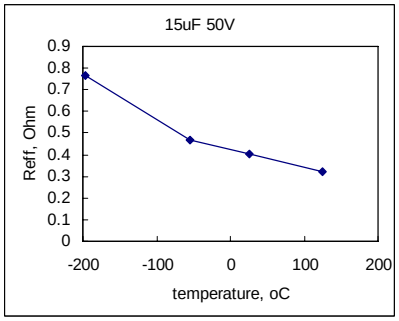

c) Variation of the effective resistance calculated per (b) with temperature

Figure II.12. Effect of temperature on results of 3SCT for 15 µF 50 V capacitors.

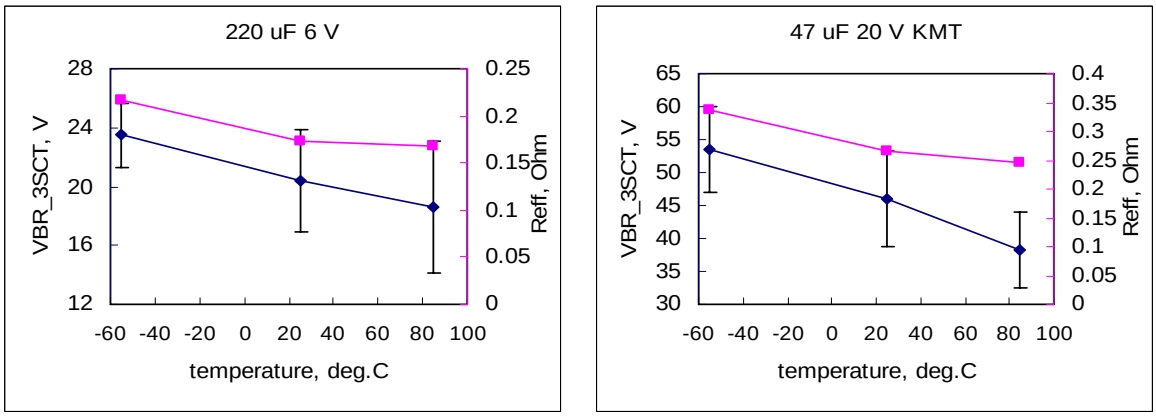

Figure II.13. Variations of 3SCT breakdown voltages and effective resistances with temperature for 220 µF/6 V (a) and 47µF/20 V KEMET (b) capacitors.

As the temperature increased from -55 ^{o}C to +85 ^{o}C the breakdown voltages decreased approximately 20% to 30% for 220 µF/6 V and 47 µF/20 V capacitors. For 15 µF /50 V capacitors, VBR_3SCT decreased ~12% as temperature increased from room temperature to 125 ^{o}C. However, low temperatures for this part resulted in a decrease of the breakdown voltages on ~5% at -55 ^{o}C and on ~12% at -196 ^{o}C compared to room temperature.

To analyze the effect of temperature on distributions of 3SCT breakdown voltages, an Arrhenius-Weibull model was used. Figure II.14 shows Weibull distributions normalized to room temperature conditions using ALTA PRO software. The results indicate a reasonably good fit of the model, thus allowing for calculation of the effective activation energies, Ea. The values of Ea were relatively small and varied from 0.0074 eV for 220 µF/6 V capacitors to 0.015 eV for 47 µF/20 V parts. Calculations based on RT and 125^{o}C data for 15 µF/50 V parts yield Ea = 0.012 eV. These results show that the activation energy of surge breakdown voltages is much less than was suggested by Moynihan [13].

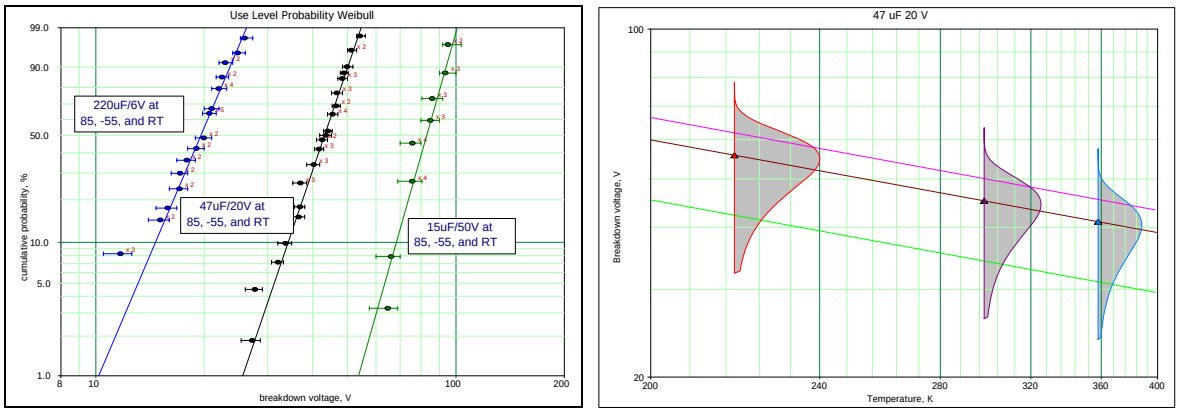

a) b)

Figure II.14. Application of Arrhenius-Weibull model for description of temperature dependencies of 3SCT breakdown voltages. Figure (a) presents Weibull distributions of all data recalculated to room temperature conditions and Figure (b) shows distributions of breakdown voltages for 47 µF/20 V at different temperatures.

VIII.7 Highly accelerated life test.

The life test was performed at conditions similar to the Weibull grading test per MIL-PRF-55365. However, to precipitate more failures, the test temperature was increased from 85 ^{o}C to 125 ^{o}C, the stress voltage was 1.5*VR, and the threshold current to determine the failure was reduced from 1 A to 2 A required per the MIL standard to 0.125 A. Note that per MIL-PRF-55365 the accelerating factor of the Weibull grading test at 1.53*VR is 20,000. Obviously, acceleration factor at 125 ^{o}C will be even greater, so a 100 hour test at 125 ^{o}C and V = 1.5 VR would be equivalent to testing for more than 230 years at the rated voltage and 85 ^{o}C.

The parts intended for life testing were soldered onto FR4 boards in groups of 16 samples, as shown in Figure II.15a, and each capacitor was connected to a power supply through fast-acting fuses, PN 0273.125H manufactured by Littelfuse and rated to 125 V and 125 mA. The nominal cold resistance of the fuses is 1 Ohm, which is in compliance with MIL-PRF-55365, and the nominal rating condition, I^2t, is 0.000691 A^2-sec. The average time current curves for the fuses are shown in Figure II.15b and indicate that that for pulses of less than ~ 1 ms, which are typically expected during failure events, the 125 mA fuses will blow at currents exceeding 0.8A. Note also, that employment of 2 A fuses per MIL-PRF-55365, at these conditions would result in failures only for parts experiencing spikes of more than ~ 15 A, whereas parts having spikes of a few amperes would not be detected and if their characteristics after the test are within the specified limits, these parts would be considered as acceptable.

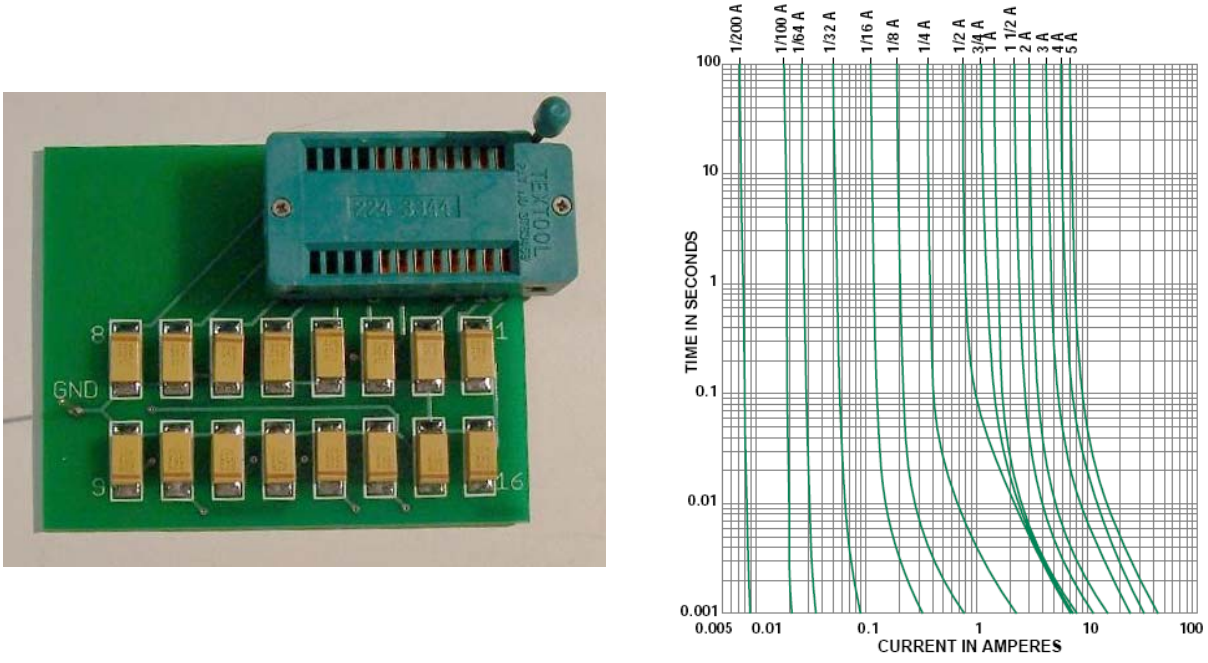

a) b)

Figure II.15. A board with 16 parts used for life testing (a) and average time current curves of the 0273 series fast-acting fuses (b). Note that for life testing 0.125 A fuses were used.

III. Distributions of 3SCT breakdown voltages.

Groups from 20 to 65 samples of different part types were tested to determine their surge current breakdown voltages, VBR-3SCT, using a technique described in the previous section. The data were approximated with Weibull and normal distributions using Weibull-6 ReliaSoft software. Results of this analysis are shown in Table III.1, where parameters of the distributions (the characteristic breakdown voltage, η, and shape parameter, β, for Weibull distributions and mean value and standard deviation, STD, for normal distributions) are presented together with characteristics allowing for choosing the best-fit type of distribution.

The chi-square test, likelihood function, LK, and correlation coefficient, ρ, were used to assess the closeness of the data to a specific distribution. The lesser the Chi-squared goodness of fit, the greater the negative values of the logarithm of the likelihood function is, and the closer ρ to 1, the better the fit. Comparison of these parameters for Weibull and normal distributions shows that according to Chi-squared characteristics, the Webull function provides a somewhat better fit. However, log(LK) and ρ indicate that both distributions can be used to describe surge current breakdown voltages. Considering that results of breakdown voltage measurements are typically displayed using Weibull plots, and statistical analysis is easier to perform using normal distributions, both distributions are used in the following analysis as appropriate.

Table III.1. Analysis of statistics of the 3SCT results.

Part	units	Distribution:	β/STD	η/mean	Chi squared goodness of fit	Log likelihood function	ρ, correlation coefficient
330 μF 10 V	26	Weibull	7.87	11.54	5.00E-04	-49.66	0.97
		Normal	1.68	10.79	1.40E-03	-48.85	0.99
33 μF 35 V	25	Weibull	11.16	69.83	4.40E-03	-56.39	0.98
AVX		Normal	7.2	66.38	1.22E-02	-57.26	0.98
33 μF 35 V	28	Weibull	14.34	74.89	5.80E-02	-58.38	0.99
KEMET		Normal	5.77	71.96	7.94E-02	-60.03	0.98
47 μF 20 V	23	Weibull	8.36	34.96	2.44E-02	-34.92	0.98
AVX		Normal	5.38	33.29	3.24E-02	-33.64	0.99
47 μF 20 V	65	Weibull	5.46	43.43	1.30E-03	-110.25	0.98
KEMET		Normal	8.87	40.15	1.80E-03	-112.62	0.98
100 μF 16 V	43	Weibull	5.45	30.06	3.72E-01	-33.28	1.00
		Normal	6.24	27.8	4.25E-01	-33.74	0.99
220 μF 6 V	36	Weibull	5.26	21.54	8.81E-05	-66.25	0.98
		Normal	4.52	19.85	2.00E-04	-66.07	0.99
15 μF 50 V	20	Weibull	8.53	78.85	1.5E-1	-44.22	0.98
		Normal	10.77	74.62	1.8E-1	-44.1	0.99
22 μF 35 V	33	Weibull	5.76	62.49	1.60E-2	-101.72	0.99
		Normal	11.12	57.94	1.36E-2	-101.96	0.99
15 μF 35 V	39	Weibull	6.97	70.25	6.01E-07	-80.79	0.98
		Normal	10.86	65.34	3.44E-05	-81.73	0.98

A Weibull plot showing distributions of the breakdown voltages for different part types is presented in Figure III.1. The results apparently confirm the applicability of the Weibull function to characterize VBR-3SCT distributions.

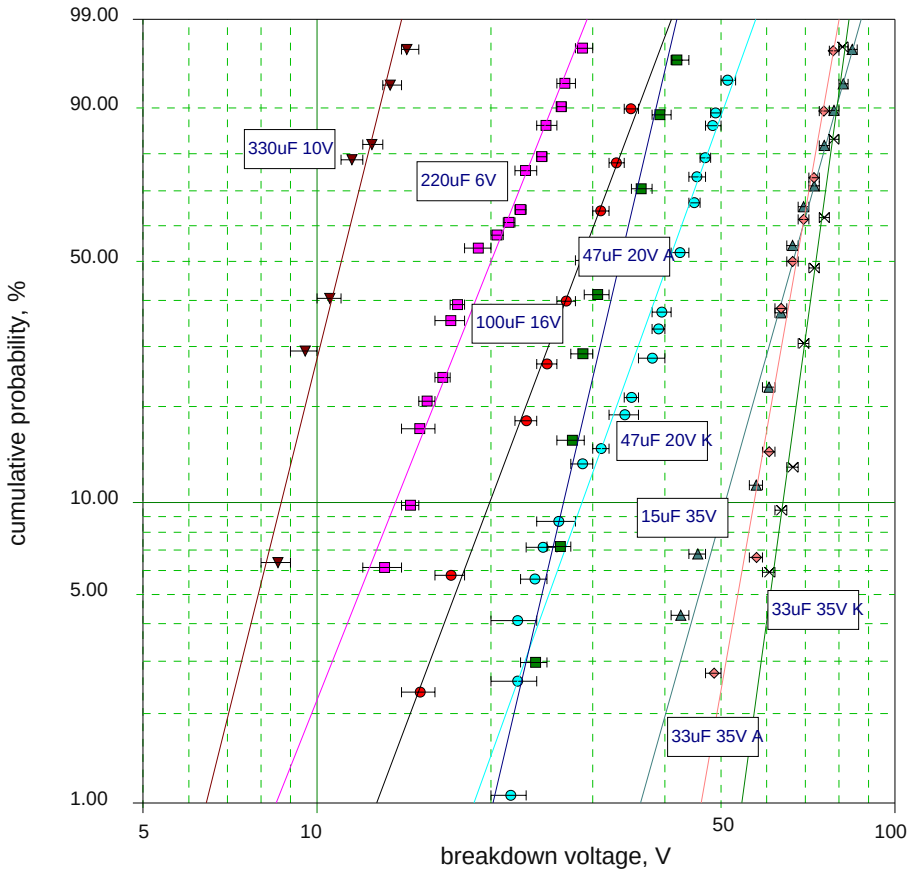

Figure III.1. Weibull plot of breakdown voltages measured on different part types during step stress surge current testing.

To analyze correlation between the rated voltage and VBR-3SCT, Weibull characteristics were normalized to the rated voltage. Results of this analysis are shown in Table III.2 and indicate that the characteristic breakdown voltage exceeds the rated voltage on average in two times. However, the spread of this ratio is large and varies from 1.2 for 330 µF/10 V capacitors to 3.6 for 220 µF/6V capacitors, resulting in a situation in which parts with lower VR have much higher breakdown voltages than parts rated to a greater voltage. This means that generally, the rated voltage is not an indicator of the robustness of the parts in surge current environments. Figure III.2 shows that there is no correlation between the rated voltage and the characteristic surge current breakdown voltage normalized to VR or the shape factor.

The shape factors averaged to 7.9 with a spread from 5.2 to 14.3. However, for most of the lots β grouped in the range from 5.2 to 8. Due to a large variation of η and β, an estimated proportion of failures at the rated voltage, F, varied in a wide range from 7.5E-4% to 25%.

Table III.2. Characteristics of Weibull distributions normalized to the rated voltage (F is the calculated proportion of failures at VR)

Part	VR, V	η, V	η/VR	β	F, %
330 μF 10 V	10	11.54	1.2	7.87	25.5
33 μF 35 V, AVX	35	69.83	2.0	11.16	0.01
33 μF 35 V, KEMET	35	74.89	2.1	14.34	0.00075
47 μF 20 V, AVX	20	34.96	1.7	8.36	0.39
47 μF 20 V, KEMET	20	43.43	2.2	5.46	0.4
100 μF 16 V	16	30.06	1.9	5.22	1.1
220 μF 6 V	6	21.54	3.6	5.26	0.15
15 μF 50 V	50	78.85	1.6	8.53	0.35
22 μF 35 V	35	62.49	1.8	5.76	0.58
15 μF 35 V	35	70.25	2.0	6.97	0.5
		average	2.0	7.9	
		STD	0.6	2.9	

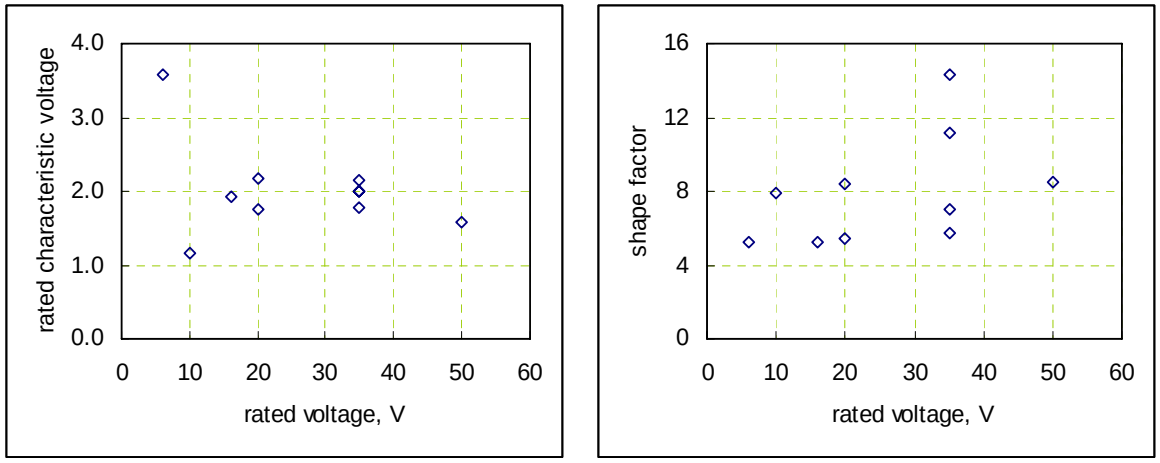

a) b)

Figure III.2. Correlation between the rated voltage and normalized characteristic breakdown voltage, VBR_3SCT/VR, (a) and shape factor (b).

Although a unimodal Weibull distribution in most cases provided a reasonably good approximation to the distributions of VBR_3SCT, in two cases it was found that the experimental data could be better described by bimodal distributions. Figure III.3 shows Weibull plots for 220 μF/6 V and 47 μF/20 V capacitors approximated with unimodal and bimodal distributions. Clearly, the latter provides a better fit, thus indicating the presence of low-breakdown-voltage and high-breakdown-voltage subgroups in these lots. Table III.3 shows parameters of distributions for the two subgroups. The difference in the characteristic breakdown voltages is rather substantial and varied from 1.5 times for 220 μF/6 V capacitors to 1.7 times for 47 μF/20 V capacitors.

Similar results suggesting that in some cases surge current breakdown voltages can be better described by bimodal Weibull distributions were reported in [3].

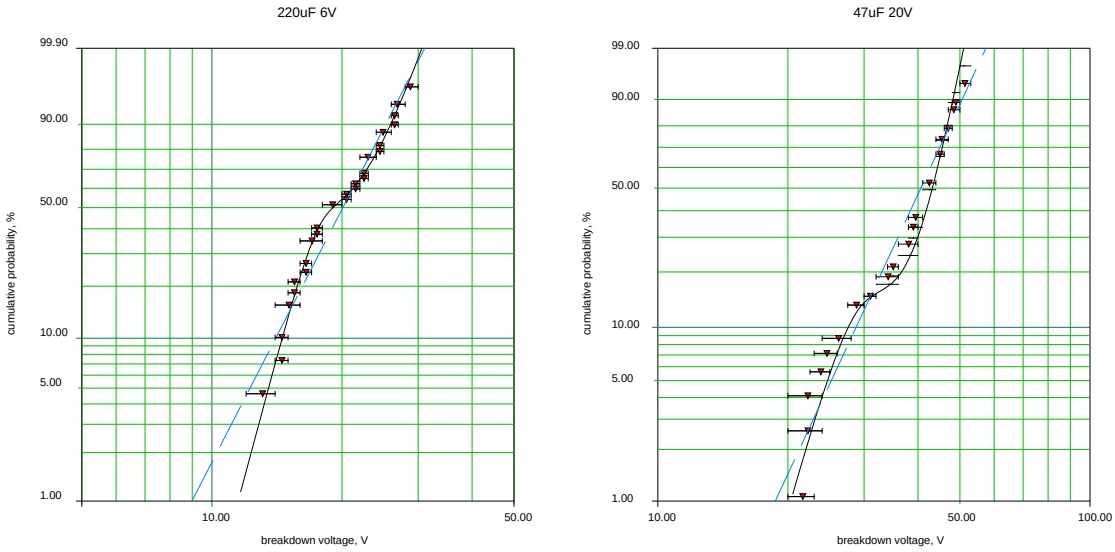

a) b)

Figure III.3. Weibull distributions of breakdown voltages for 220 μF/6 V (a) and 47 μF/20 V (b) capacitors approximated with unimodal (dashed line) and bimodal distributions.

Table III.3. Parameters of unimodal and bimodal distributions.

Part	Distribution	Proportion of gr.I	ηI	βI	ηII	βII
220 μF 6 V	unimodal	100%	21.5	5.3	-	-
	bimodal	42%	16.6	10.6	24.4	7.7
47 μF 20 V	unimodal	100%	43.4	5.5	-	-
	bimodal	14.5%	27.2	9	45.3	12.7

IV. Effect of SCT on characteristics of tantalum capacitors.

IV.1. Effect of SCT screening.

Analysis of the effect of stresses developed during SCT screening on characteristics of tantalum capacitors was carried out by measurements of characteristics of nine samples of each part type. To increase the level of stress, multiple surge current testing was used at increasing number of cycles and stress voltages exceeding VR. Measurements of capacitance, dissipation factor, ESR, and leakage currents were carried out initially, after 10 SCT cycles and V = VR, and then after additional cycling (up to 100 cycles) at voltages increased up to 2VR in some cases. Capacitance and dissipation factor were measured at 120 Hz, ESR at 100 kHz, and leakage currents at rated voltages after 5 minutes of polarization.

Results of the tests are shown in Figures IV.1 to IV.7 and indicate only minor variations of the AC and DC characteristics. Only one part in the 33 μF/35 V AVX group increased noticeably the value of DF and ESR. However, these changes occurred after 10 cycles at 65 V, which significantly (1.85 times) exceeds the rated voltage.

Results of multiple surge current tests described in following sections show that the effective resistance of SCT, R_{eff}, which is closely related to ESR, did not change significantly even after hundreds of cycles at voltages close to the breakdown. This means that the observed increase in ESR for one of 33 μF/35 V parts is probably not related to the surge current stresses and there is definitely no evidence of the effect of SCT on AC and DC characteristics of the parts at least up to stress voltages of 1.5VR.

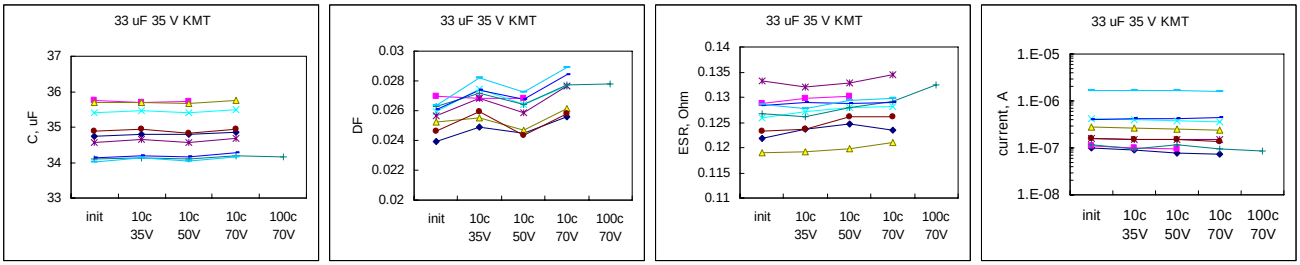

Figure IV.1. Characteristics of 33 μF/35 V KEMET capacitors sequentially after 10 cycles at 35 V and 50 V and 100 cycles at 70 V.

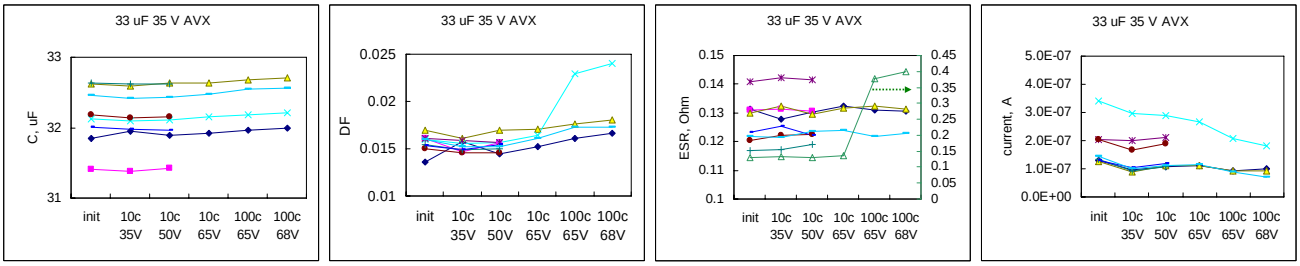

Figure IV.2. Characteristics of 33 μF/35 V AVX capacitors sequentially after 10 cycles at 35 V, 10 cycles at 50 V, 10 cycles at 65 V, 100 cycles at 65 V, and 100 cycles at 68 V.

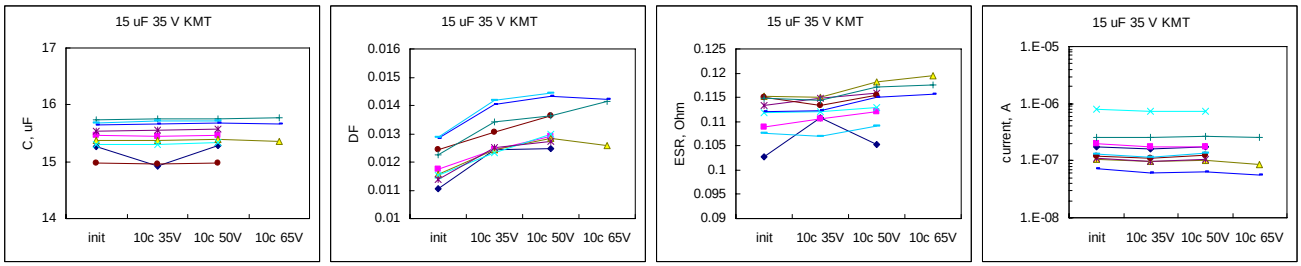

Figure IV.3. Characteristics of 15 µF/35V capacitors sequentially after 10 cycles at 35 V, 10 cycles at 50 V, and 10 cycles at 65V.

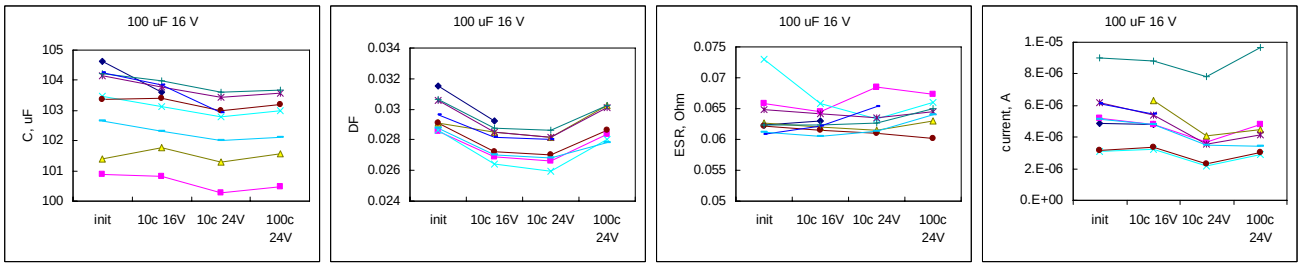

Figure IV.4. Characteristics of 100 µF/16 V capacitors sequentially after 10 cycles at 16 V, 10 cycles at 24 V, and 100 cycles at 24V.

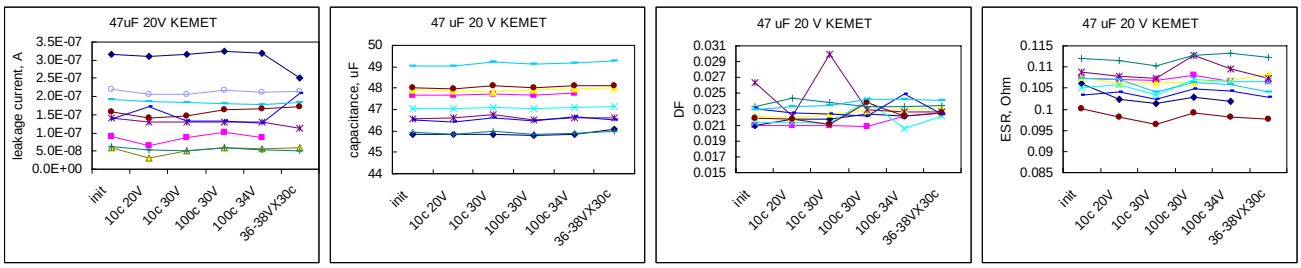

Figure IV.5. Characteristics of 47 µF/20 V, AVX, capacitors sequentially after 10 cycles at 20 V, 10 cycles at 30 V, 100 cycles at 30 V, and 30 cycles at 36/38 V.

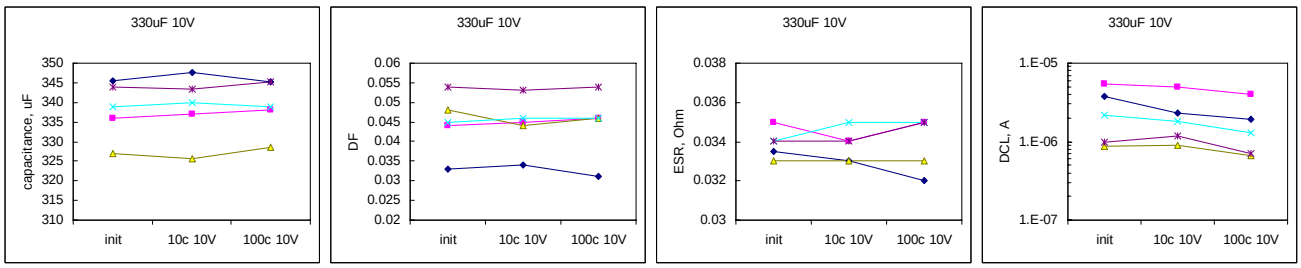

Figure IV.6. Characteristics of 330 µF/10 V capacitors sequentially after 10 cycles at 10 V and 100 cycles at 10 V (most of these parts failed testing at voltages higher than VR).

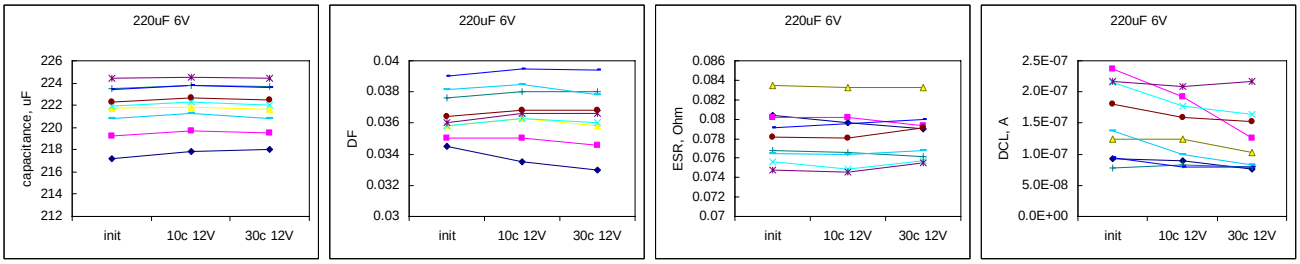

Figure IV.7. Characteristics of 220 µF/6 V capacitors sequentially after 10 SCT cycles and 30 SCT cycles at 12 V.

IV.2. Effect of multiple discharge cycles.

Two groups of 15 µF/50 V capacitors were stressed by multiple discharge current spikes (up to 7 million cycles) at charge voltages of 50 V (first group) and 60 V (second group). The amplitude of current spikes was ~ 130 A for the first group and ~150 A for the second group. Periodically, DC and AC characteristics were measured throughout these tests.

Results of these measurements are shown in Figures IV.8 and IV.9. No failures or any significant variations of AC characteristics were observed. Leakage currents first decreased with the time of testing, but then after ~ 10^5 cycles started rising and finally rose three to 10 times. Control experiments with parts tested without discharging showed that this result is not related to current spiking and is due to a long-term DC bias stress. The mechanism of this phenomenon will be discussed in the next report.

A conclusion based on results of these tests is that tantalum capacitors are capable of withstanding practically unlimited number of high current spikes at rated voltages without any degradation.

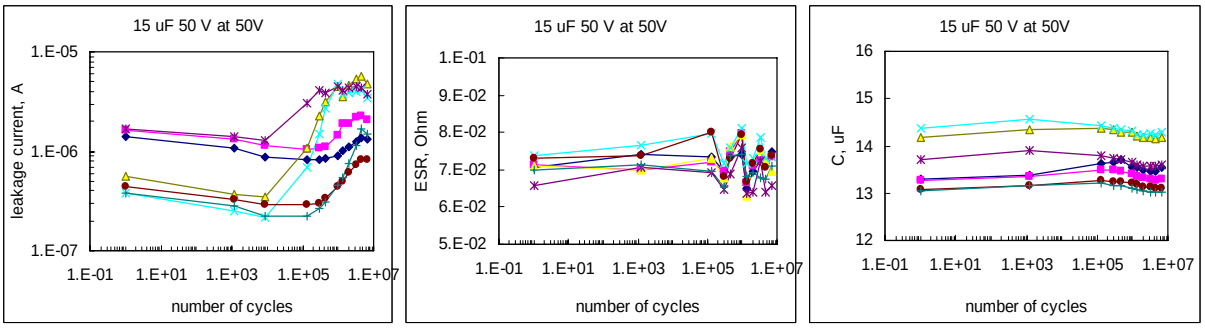

Figure IV.8. Variations of characteristics of 15 µF/50 V capacitors during multiple discharge current testing at 50 V.

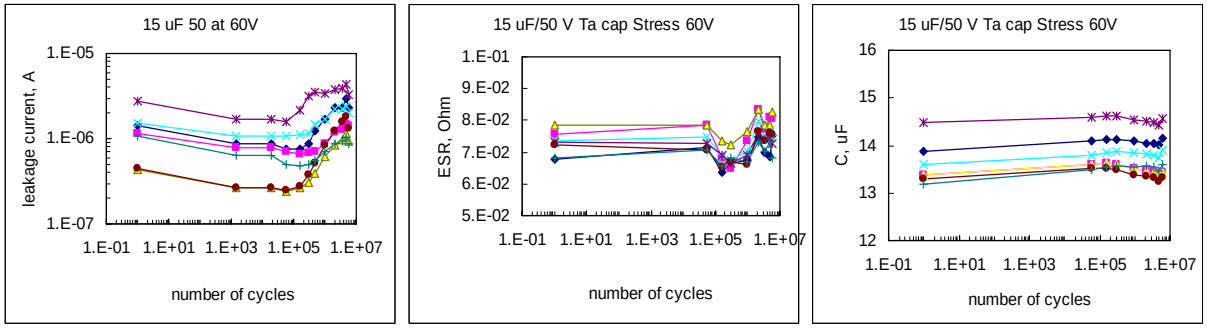

Figure IV.9. Variations of characteristics of 15 μF/50 V capacitors during multiple discharge current testing at 60 V.

V. Effect of SCT on reliability under steady-state conditions.

V.1 Life test at 125 °C

For this evaluation, groups of 32 to 50 parts were characterized initially to assure that their characteristics were within the specified limits, and then they were split into two equal subgroups. One of the subgroups was subjected to SCT (typically 10 cycles at 1.5VR) and the other used as a reference. Then the parts were soldered onto boards and tested at 125 °C and V = 1.5VR for up to 250 hrs or untill a substantial number of failures occur. Power supply currents and number of failures (blown fuses) were checked and recorded periodically through the testing.

33 µF/35 V KEMET capacitors.

Sixteen parts were stressed by 10 SCT cycles at 50 V each and soldered onto the board together with a control group of 16 non-stressed parts. The life test was carried out at 50 V, 125 °C for 168 hours. Results of this test are plotted in a Weibull diagram in Figure V.1 and suggest that parts with SCT screening had a somewhat lesser number of failures. However, the Fisher exact test showed no significant difference in the proportion of failed parts in these two groups.

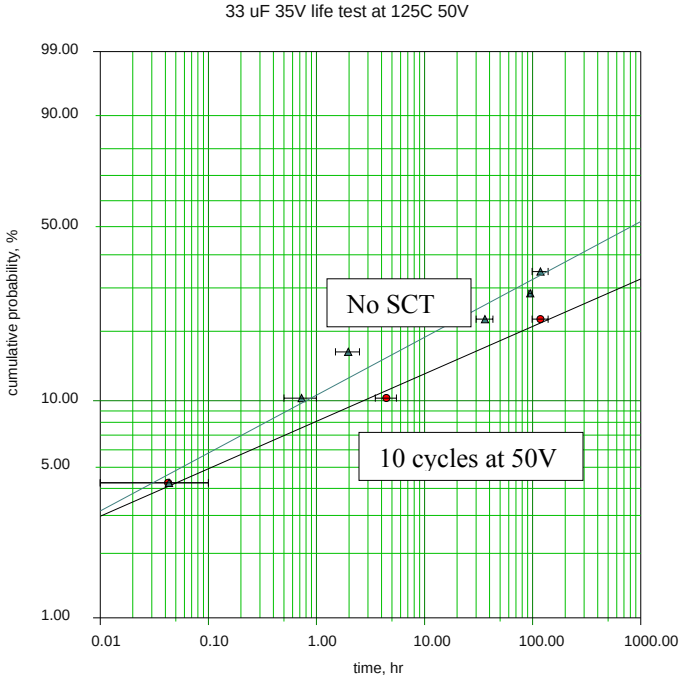

Figure V.1. Results of life testing of 33 µF/35 V KEMET capacitors at 50 V, 125 °C.

33 µF/35 V AVX capacitors.

These parts were tested similarly to the previous groups, but the life test at 125 °C and 50 V was extended to 250 hours to precipitate more failures. Results of the testing are shown in a Weibull diagram in Figure V.2 and indicate a larger proportion of failures (~60% in the first group and ~40% in the second group) by the end of the test. Similar to the previous test, parts screened by

10 SCT cycles at 50 V had a lesser number of failures. However, the statistical analysis did not reveal a significant difference in the results. This allows considering both groups for a reliability assessment of the lot. A distribution of failures for all 33 μF/35 V AVX tested samples is shown in Figure V.2.b. This distribution features a relatively low failure rate during the first 10 hours and an increased rate of failures after this time. The times to failure can be more accurately described by a bimodal Weibull distribution. Parameters of these distributions are shown in Table V.1. The first group has a shape factor $\beta < 1$, thus indicating infant mortality failures, whereas the second group has $\beta > 1$, which is an indicator of wear-out failures. The possibility of wear-out failures in tantalum capacitors will be discussed in the next report.

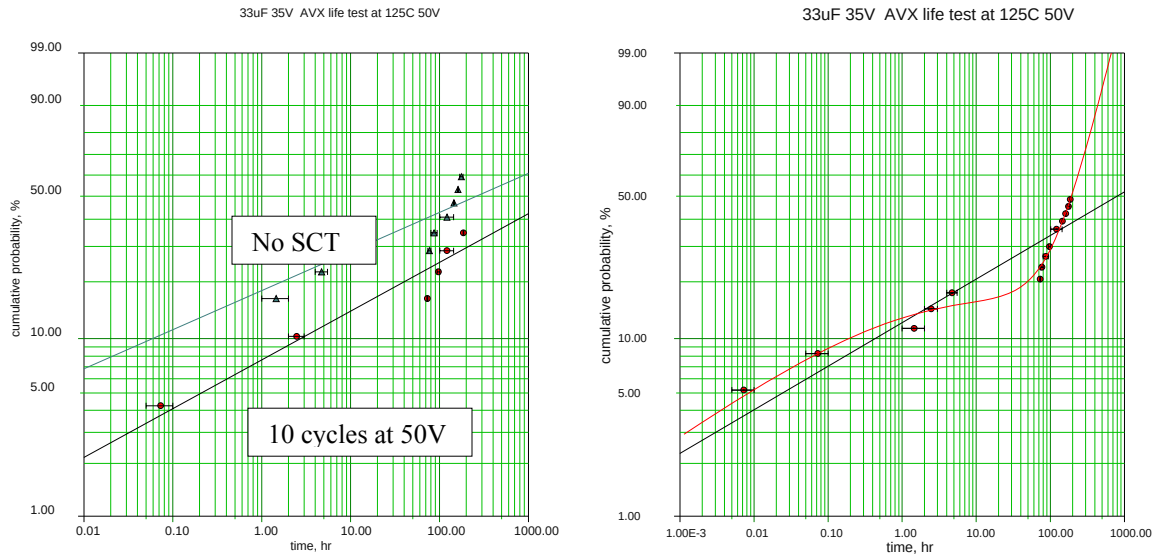

a) b)

Figure V.2. Results of life testing of 33 μF/35 V AVX capacitors at 50 V, 125 °C for parts with and without SCT screening (a). Figure (b) shows combined results of the testing for two groups approximated with unimodal (black line) and bimodal (red line) distributions.

Table V.1. Parameters of Weibull distributions for 33 μF/35 V AVX capacitors.

Distribution	β1	η1	β2	η2	Proportion of 1st group
Unimodal	0.25	3442	-	-	100%
Bimodal	0.31	0.21	1.73	282	16%

47 μF/20 V KEMET capacitors.

For this testing, 16 parts were stressed by 10 SCT cycles at 30 V (1.5VR) and then tested together with 16 control parts at 125 °C, 30 V, for 168 hours. Results of the test are shown in Figure V.3 and suggest that similar to previous cases, parts with SCT screening demonstrated a somewhat lower (although not statistically significant) failure rate.

An interesting phenomenon was observed during life testing: power supply currents increased with time of the testing at 125 °C (see Figure V.3.b). The significance of these data will be discussed in the future.

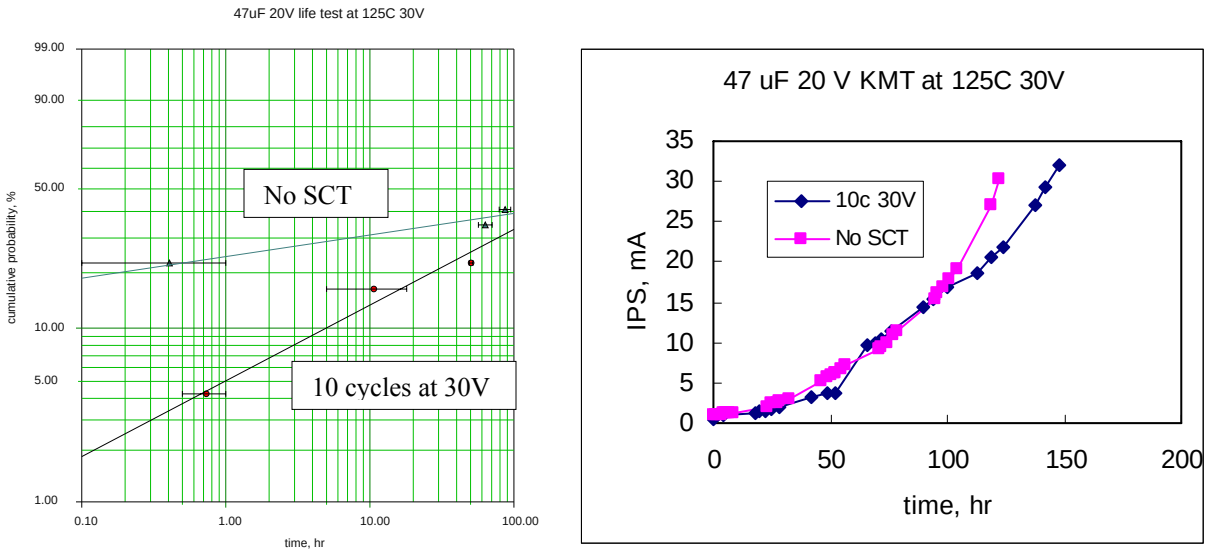

a) b)

Figure V.3. Results of life testing of 47 µF/20 V KEMET capacitors at 30 V, 125 °C (a) and variation of power supply currents during the test (b).

100 µF/16 V capacitors.

These parts were tested at 120 °C, 24 V in two groups of 25 samples each, with the first group stressed by 10 SCT cycles at 16 V. The duration of the test was 72 hours only because of the high rate of failures as shown in Figure V.4. In this lot, in spite of relatively mild SCT stress conditions (screening at rated voltage), parts with SCT had a somewhat higher level of failures. However, the difference between the two groups was not statistically significant.

220 µF/6 V capacitors.

Life testing of these parts was carried out on two 16-sample groups at 125 °C and 9V for 168 hours. Prior to the testing the first group was subjected to 10 SCT cycles at 9V. No failures were detected in the second group, and one part failed after 164 hours in the first group. These results are not statistically different per the Fisher exact test. Interestingly, the failed part had normal electrical characteristics, which did not change significantly compared to the initial values. Similar results, indicating that parts failing life testing appeared to be normal based on post-test measurements, were observed in other lots, and possible reasons for this will be discussed in the next report.

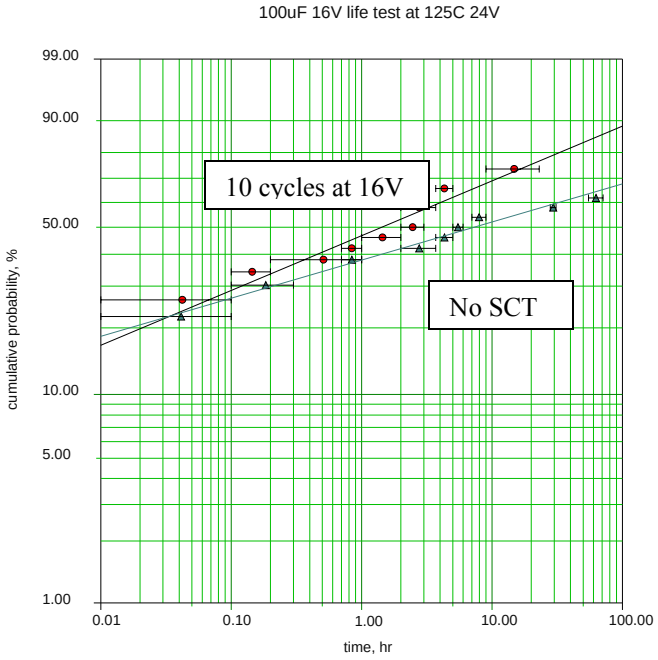

Figure V.4. Results of life testing of 100 μF/16 V capacitors at 24 V, 125 °C.

A summary of life test results, including test conditions, quantity of failed parts, Weibull characteristics of the relevant life time distributions, and p-values of the Fisher exact test are shown in Table V.2. The p-value indicates a statistical significance of difference between the proportions of failed parts. Typically, the difference can be considered as significant if $p < 0.05$. Analysis of the results indicates that SCT screening even at voltages of 1.5VR does not cause additional failures during 125 °C life testing. Interestingly, the values of the shape parameter, β, calculated in the assumption of unimodal Weibull distributions, were less than 1, indicating that most observed failures are infant mortality failures caused by some manufacturing-induced flaws in the part.

Table V.2. Summary of life test results at 125 °C

Part	Life Test Condition	Precondition	QTY	Failures	Weibull Distr.		Fisher Exact
					η, hr.	β	
100 μF/16 V	24V, 72 hr	w/o SCT	25	16	52.4	0.19	0.82
		SCT 16 V, 10c	25	19	5.6	0.27	
220 μF/6 V	9V, 168 hr	w/o SCT	16	0	-	-	1
		SCT 9 V, 10c	16	1	-	-	
47 μF/20 V KEMET	30V, 168 hr	w/o SCT	16	7	24102	0.13	0.74
		SCT 30 V, 10c	16	5	779	0.44	
33 uF/35 V AVX	50V, 250 hr	w/o SCT	16	10	1337	0.22	0.54
		SCT 50 V, 10c	16	6	8487	0.28	
33 μF/35 V KEMET	50V, 168 hr	w/o SCT	16	6	3153	0.27	0.72
		SCT 50 V, 10c	16	4	65780	0.22	

As SCT screening is not a significant factor, results obtained for the two tested groups in each part type (with and without SCT screening) were combined to obtain a more statistically significant results of testing at 125 ^{o}C. These results are presented in a Weibull plot in Figure V.5, and the respective characteristics of the distributions are shown in Table V.3.

Parameters of a Weibull distribution for 220 µF/6 V capacitors could not be calculated because only one part failed. However, the shape parameters for other lots varied in a relatively narrow range, from 0.2 to 0.29. This allows for an assumption that the 220 µF/6 V parts would also have a value in this range and by setting $\beta = 0.25$, the value of η was calculated to accommodate one failure after 164 hours. With this estimation the range of the characteristic times to failure spreads over a wide range of more than 8 orders of magnitude, from 10 to ~ 10^9 hours, thus reflecting a significant difference in the reliability of different part types.

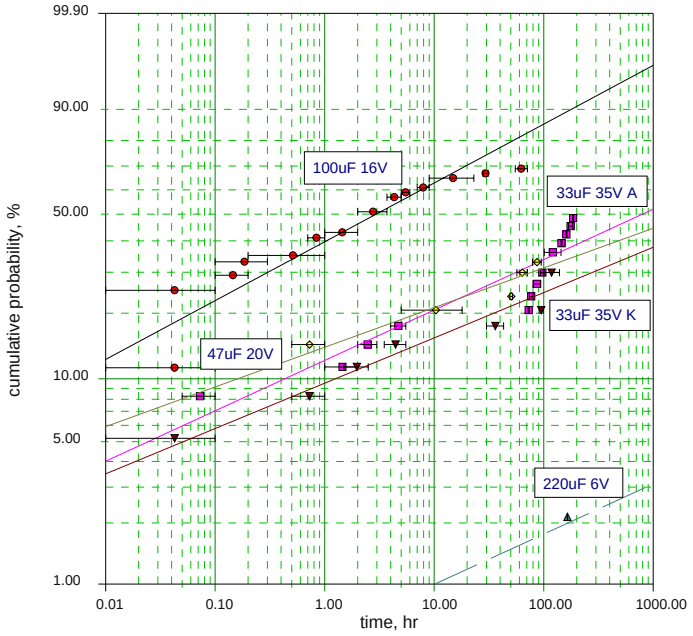

Figure V.5. Distributions of time-to-failure during life testing at 125 ^{o}C and V = 1.5VR for different types of capacitors.

Table V.3. Combined life test data.

Part	Life Test Condition	QTY	Failures	Weibull Distribution	
				η, hr	β
100 µF/16 V	24V, 72 hr	50	25	10.3	0.29
220 µF/6 V	9V, 164 hr	32	1	1E9*	0.25*
47 µF/20 V KEMET	30V, 162 hr	32	12	1.5E4	0.2
33 µF/35 V AVX	50V, 251 hr	32	16	3.4E3	0.25
33 µF/35 V KEMET	50V, 167 hr	32	10	2.7E4	0.22

* estimated values.

V.2 Life test at room temperature.

This test was carried out by monitoring leakage currents at room temperature and V = 2VR for up to 200 hours. Two subgroups of different part types, with 9 to 18 samples each, were used. To simulate SCT screening, one of the subgroups was stressed by multiple (N_c = 10 to 30) cycles at voltages in the range from 1.25VR to 2VR, and another was comprised of unscreened parts.

During RT life testing, the voltage was applied to each sample via a 1 kOhm resistor, and the currents were measured and recorded by a PC-based data-capturing system every 10 seconds. A failure event was detected and recorded when a scintillation current spike occurred. It was assumed that similar spikes caused failures during 125 ^{o}C life testing. However, contrary to room temperature testing, the currents during 125 ^{o}C testing were not limited with a resistor thus sustaining the scintillation breakdown and causing the fuse to blow.

Test results for different part types are show in Figures V.6 to V.9 and are summarized in Table V.4. Statistical analysis of the test results, similar to life testing at 125 ^{o}C, showed no difference in the proportion of life test failures (scintillations) in parts stressed and non-stressed by surge current test screening.

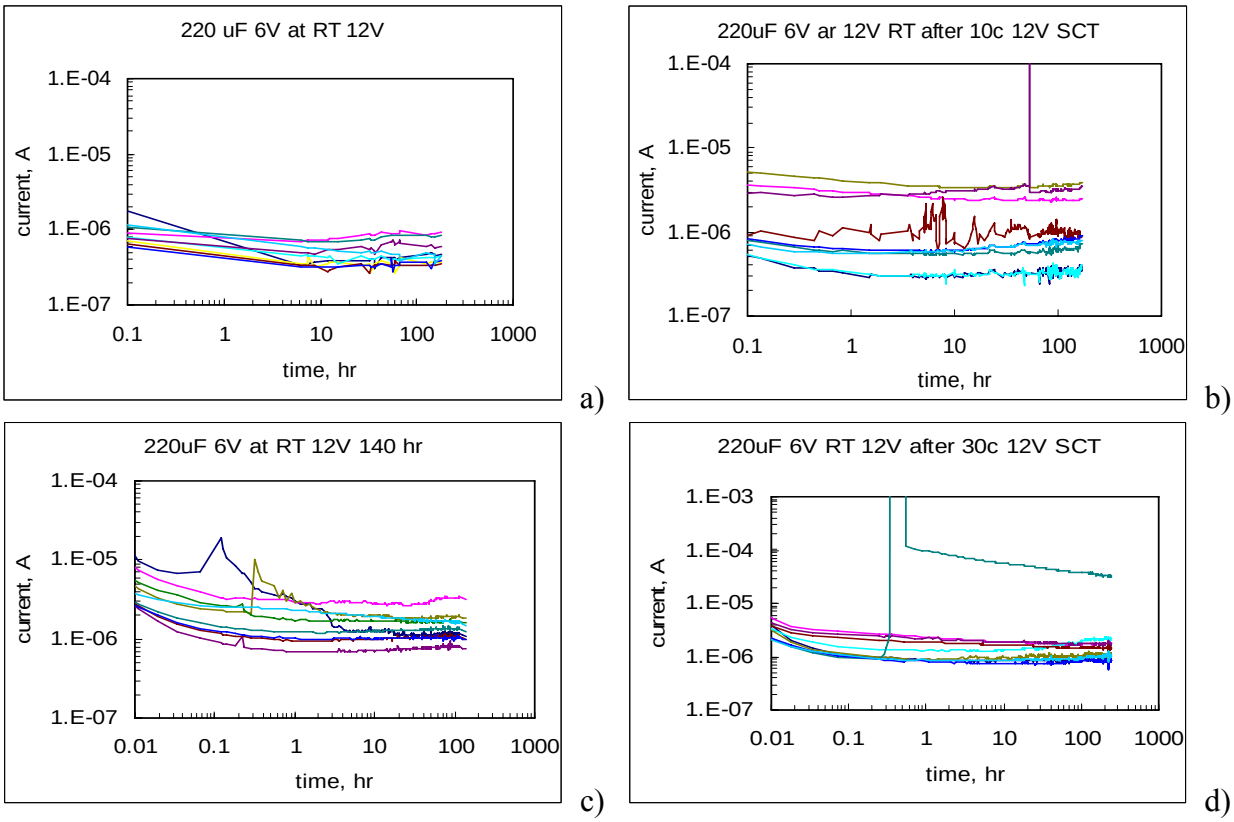

Figure V.6. Variations of leakage currents with time at room temperature, 12 V for 220 µF/6 V capacitors. Figures (b) and (d) show subgroups stressed by 10 (b) and 30 (d) SCT 30 cycles at 12 V and indicate 3 samples out of 18 with scintillations. Figures (a) and (c) show results for non-stressed parts, with two parts out of 18 having scintillation breakdowns.

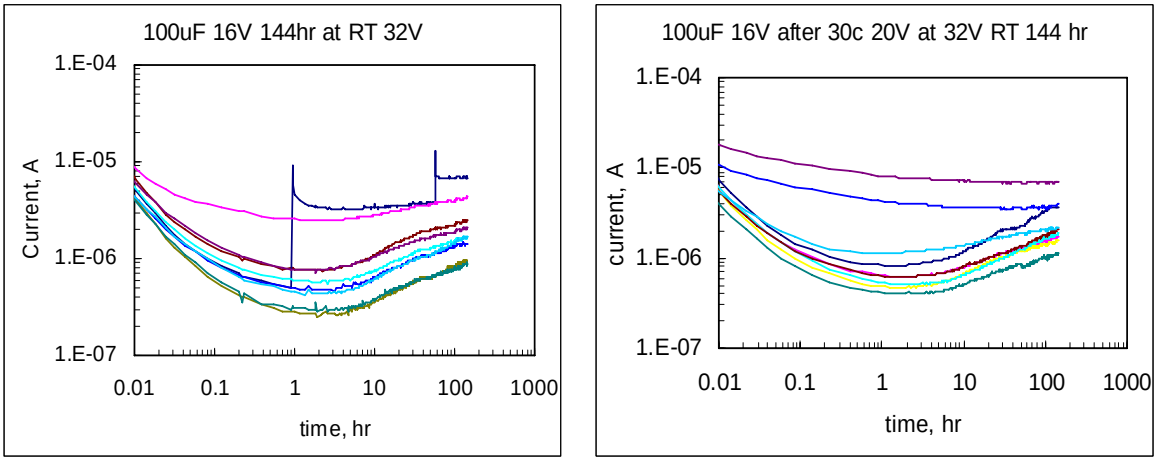

a) b)

Figure V.7. Variations of leakage currents with time at room temperature, 32 V for 100 µF/16 V capacitors. Figure (a) show a non-stressed subgroup and Figure (b) shows a subgroup stressed by 30 SCT 30 cycles at 32V. Note that only one sample in the non-stressed group out of 9 had repeat scintillations after ~ 1 hour and then after ~80 hours of testing.

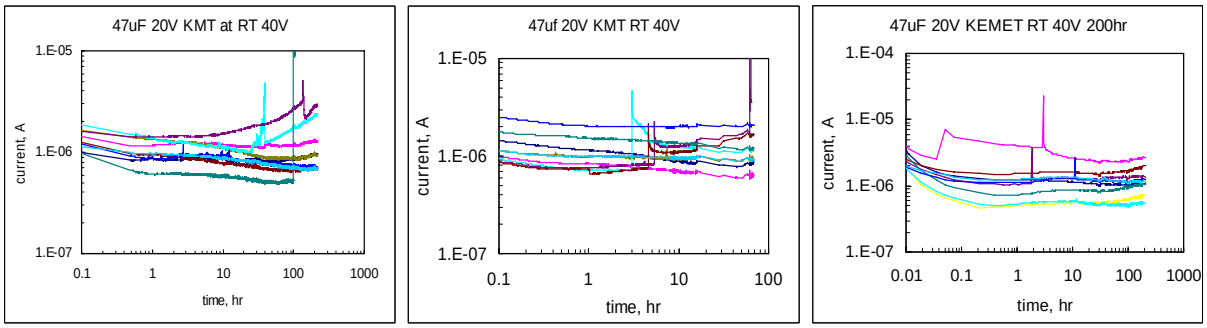

a) b) c)

Figure V.8. Leakage currents in 47 µF/20 V KEMET capacitors during room temperature life testing at 40 V. Out of 18 non-stressed parts, shown in Figures (a) and (c), six samples had scintillations. Out of nine parts screened with 10-cycle SCT at 40 V (b), three samples had scintillations.

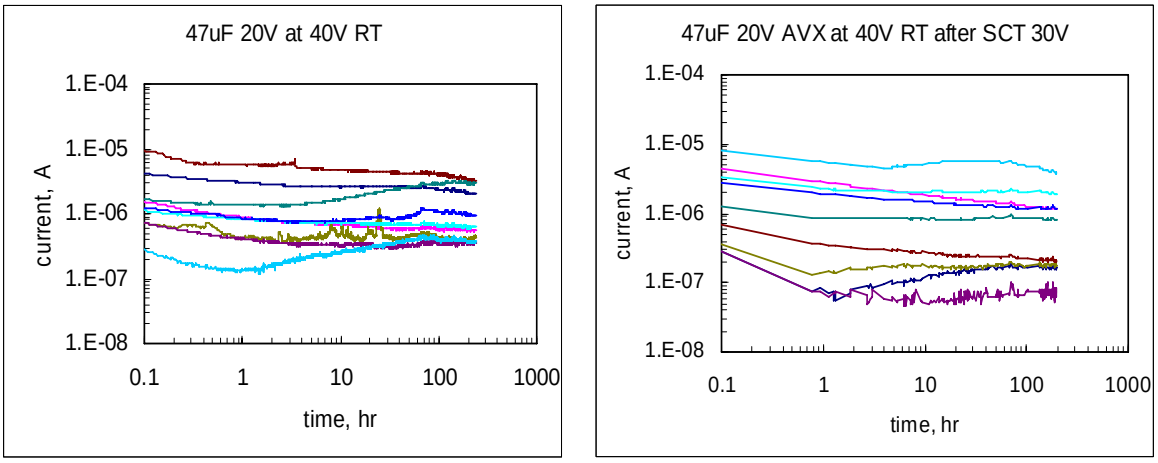

a) b)

Figure V.9. Leakage currents in 47 µF/20 V AVX capacitors during room temperature life testing at 40V. No failures were observed in a subgroup of nine samples stressed by 10-cycle SCT at 30 V (b), and one out of nine parts had scintillations in a subgroup (a), tested without SCT screening.

Table V.4. Summary of life test results at RT

Part	Life Test Condition	Precondition	QTY	Failures
100 µF/16 V	32 V, 144 hr	w/o SCT	9	1
		SCT 20 V, 30c	9	0
220 µF/6 V	12 V, 200 hr	w/o SCT	18	2
		SCT 12 V, 10c	18	3
47 µF/20 V KEMET	40 V, 200 hr	w/o SCT	18	6
		SCT 40 V, 10c	9	3
47 µF/20 V AVX	40 V, 200 hr	w/o SCT	9	1
		SCT 30 V, 10c	9	0

VI. Effect of life testing on results of SCT.

To reveal a possible effect of life testing on surge current breakdown voltages, parts from seven different lots were subjected to 3SCT after life testing at 1.5VR and 125 ^{o}C and after long-term bias at room temperature. Samples both passing and failing life tests were used. However, only parts having acceptable characteristics were selected for 3SCT and further analysis.

Results described in the previous section indicate that there is no evidence that SCT screening affects results of life testing. For this reason, it can be assumed that SCT screening before life testing does not affect results of post-life 3SCT. This allows dividing all parts after life testing into two groups only: one with samples passing life test, and another with samples failing the test.

Average breakdown voltages and standard deviations measured during post-life 3SCT for different part types are presented in Tables VI.1 to VI.7. For reference, these tables show also results obtained using unstressed devices.

Table VI.1. Surge current breakdown voltages of 220 μF/6 V capacitors.

Condition	QTY	Average	STD
unstressed	36	19.85	4.52
passed 168hr 125C 9V	16	20.62	2.6
failed 168hr 125C 9V	1	20	-
passed 168hr RT 12V	15	24.13	3.89
failed 168hr RT 12V	2	19	1.4
passed 240hr RT 12V	13	22.38	3.64
failed 240hr RT 12V	5	20.6	1.67

All 220 μF/6 V parts after 125 ^{o}C life testing, both passed and failed, had breakdown voltages which did not change significantly compared to unstressed parts. However, for the parts after RT life testing the breakdown voltages were ~10% higher.

Table VI.2. Surge current breakdown voltages of 100 μF/16 V capacitors.

Condition	QTY	Average	STD
unstressed	29	27.99	6.31
passed 125C 72hr 24V	10	28.80	5.90
failed 125C 72hr 24V	27	26.52	5.25
passed RT 144hr 32V	17	32.47	6.18
failed RT 144hr 32V	1	38.00	-

No significant effect of life testing at 125 ^{o}C was observed for 100 μF/16 V parts; whereas long-term room temperature testing at 32 V increased breakdown voltages on ~ 15%. Note that one part failing RT testing due to two scintillations had 3SCT breakdown voltage ~2.4 times exceeding the rated voltage. This might be used as an indication that the proofing of the parts is effective: simulation of a scintillation breakdown by proofing at high voltage, V_{proof} = 32 V, through a 1 kOhm resistor apparently trigged scintillation, self-healed the part, and prevented

surge current failure at 32 V (the part failed at 38 V). However, other results of the testing are not consistent with this hypothesis. For example, out of 17 parts that passed 144 hour test at 32 V, seven samples failed surge current test at voltages below 32V. This means that the sustained scintillation theory, which is a justification for the proofing technology, is not valid and parts, that were proven to have no scintillations at $V = V_{proof}$, still might fail surge current testing at this voltage.

Table VI.3. Surge current breakdown voltages of 33 μF/35 V AVX capacitors.

Condition	QTY	Average	STD
unstressed	25	66.38	7.20
passed 250hr 125C 50V	8	66.12	13.79
failed 250hr 125C 50V	12	66.5	9.09

Table VI.4. Surge current breakdown voltages of 33 μF/35 V KEMET capacitors.

Condition	QTY	Average	STD
unstressed	28	71.96	5.77
passed 168hr 125C 50V	14	71.43	9.25
failed 168hr 125C 50V	9	73	5.61

Both 33 μF/35 V parts manufactured by AVX and KEMET manifested no significant effect of 125 ^{o}C life testing at 1.5VR on the distributions of the surge current breakdown voltages.

Table VI.5. Surge current breakdown voltages of 47 μF/20 V AVX capacitors.

Condition	QTY	Average	STD
unstressed	23	33.29	5.38
passed 200hr RT 30 V	17	40.82	5.56
failed 200hr RT 30 V	1	38	

Similar to results obtained for 100 μF/16 V capacitors, 47 μF/20 V AVX parts demonstrated a significant (~20%) increase of the breakdown voltages after room temperature life testing. One part having scintillations during the testing had a breakdown voltage 1.8 times exceeding the rated one, confirming that self-healed scintillations do not degrade the capability of the parts to withstand surge current conditions.

Table VI.6. Surge current breakdown voltages of 47 μF/20 V KEMET capacitors.

Condition	QTY	Average	STD
unstressed	65	40.15	8.87
passed 168hr 125C 30 V	20	41.60	6.64
failed 168hr 125C 30 V	12	38.75	9.14
passed 200hr RT 40 V	15	46.80	8.37
failed 200hr RT 40 V	3	39.00	9.16

Testing of 47 μF/20 V KEMET capacitors did not reveal any significant effect of 125 °C life testing on results of 3SCT. However, room temperature life test resulted in ~ 16% increase in VBR_3SCT. Parts failed life testing at 125 °C and RT had breakdown voltages similar to the unstressed parts.

Table VI.7. Surge current breakdown voltages of 15 μF/35 V capacitors.

Condition	QTY	Average	STD
unstressed	39	65.34	10.86
passed 125hr RT 50 V	9	65.67	13.6

Surge current breakdown voltages in 15 μF/35 V parts stressed by 50 V at RT for 125 hours and unstressed parts were practically identical.

All test results are summarized in Tables VI.8 and VI.9 and allow the following conclusions:

1. There is no significant effect of life testing at 125 °C on surge current breakdown voltages.
2. Room temperature long-term stress of the parts at high voltages (~2VR) might increase VBR_3SCT on 10% to 20%.
3. Scintillation breakdown does not degrade the capability of the parts to withstand surge current conditions. However, "proofing" of the parts at high voltages does not guarantee that the part would withstand this voltage under surge current conditions.

Table VI.8. Summary of test results on the effect of life testing on VBR_3SCT

Part	Effect of life test at 125 °C, 1.5VR	Effect of life test at RT, 1.5VR	Effect of life test at RT, 2VR
220 μF/6 V	no effect	-	increase 10 to 20%
100 μF/16 V	no effect	-	increase ~15%
33 μF/35 V AVX	no effect	-	-
33 μF/35 V KMT	no effect	-	-
47 μF/20 V AVX	-	increase ~20%	-
47 μF/20 V KMT	no effect	-	increase ~15%
15 μF/35 V	-	no effect	-

Table VI.9. Summary of test results on the effect of life test failures on VBR_3SCT

Part	Failures during life test at 125 °C, 1.5VR	Failures during life test at RT, 1.5VR
220 μF/6 V	-	-
100 μF/16 V	no effect	-
33 μF/35 V AVX	no effect	-
33 μF/35 V KMT	no effect	-
47 μF/20 V AVX	-	-
47 μF/20 V KMT	no effect	
15 μF/35 V	-	no effect

VII. Failures during multiple surge current cycling.

The purpose of this section of the report is to evaluate the possibility of surge current failures at numbers of cycles exceeding 10. If a part that passed 10 cycles can fail after a few additional cycles, then SCT screening is not effective and might even increase the rate of surge current failures during applications.

To estimate the probability of failures at Nc > 10, several part types were subjected to 3SCT at multiple cycles at each voltage step. The current spike amplitude was used as an in-situ parameter indicating possible degradation in the parts. It was expected that stresses during SCT might increase ESR and/or leakage currents and thus degrade I_{sp} and increase R_{eff}.

VII.1. Effect of number of cycles on current spike amplitude.

Figure VII.1 shows typical examples of variations of current spike amplitude during 3SCT at multiple cycling at each step for 22 µF/35 V and 33 µF/35 V capacitors. It is seen that I_{sp} has some relatively minor spreading around the mean values at every step voltage, but apparently no systematic variations of I_{sp} occur.

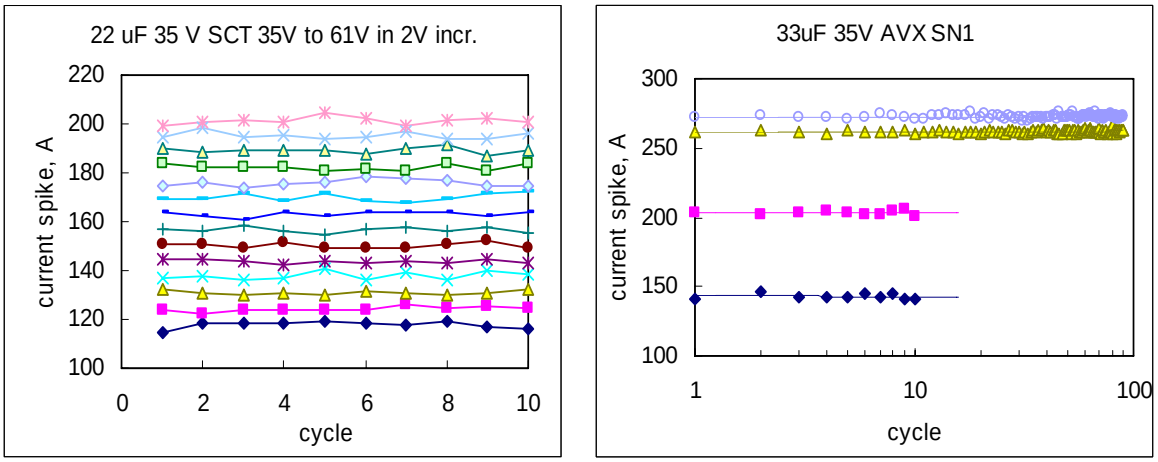

a) b)

Figure VII.1. Variations of current spike amplitudes with number of cycles during multiple cycling 3SCT for 22 µF/35 V (a) and 33 µF/35V (b) capacitors. In the first case, the test was carried out starting 35 V in 2 V increments and 10 cycles per step. In the second case, the part was stressed sequentially at 35 V and 50 V for 10 cycles, and then at 65 V and 70 V for 100 cycles.

To characterize possible variations of I_{sp} with the number of cycles more accurately, slopes of the I_{sp} - N_c plots were calculated using the best-fit linear approximation at each step stress voltage. Results of these calculations for various 35 V rated capacitors during 10-cycle-per-step test conditions are shown in Table VII.1. The table shows the quantity of tested parts, average slopes, and their standard deviations. Statistical analysis of the data shows that in all cases there is no evidence to support rejection of the "null hypothesis", which means that the average slope is not

different from zero at the significance level of 95%. Similar results were obtained for 100 μF/16 V capacitors tested at 16 V and 24 V (see Table VII.2.)

Table VII.1. Slopes (A/cycle) of Isp during 10-cycle tests at different voltages.

Part		35 V	50 V	65 V	70 V
33 μF 35 V AVX	QTY	9	9	4	3
	AVR	0.034	-0.06	-0.054	-0.00099
	STD	0.14	0.13	0.11	0.004
33 μF 35 V KMT	QTY	9	9		8
	AVR	-0.07	-0.11	-	-0.08
	STD	0.12	0.15		0.18
15 μF 35 V KMT	QTY	9	9	2	
	AVR	-0.07	-0.16	-0.23	
	STD	0.11	0.09	0.13	

Table VII.2. Slopes (A/cycle) of Isp during 10- and 100-cycle tests of 100 μF/16 V capacitors.

	16 V 10 cycles	24 V 100 cycles
QTY	9	7
AVR	2.1E-02	2.3E-03
STD	9.1E-02	4.6E-03

A 100-cycle-per-step surge current test was carried out on 47 μF/20 V, 330 μF/10 V, 220 μF/6 V, and 100 μF/16 V capacitors with seven to 14 samples in each group. Typical examples of I_{sp}-N_c variations and dependencies of the slope on the stress voltages are presented in Figures VII.2 to VII.5. The results show that even at voltages that cause breakdown after multiple cycling (the topmost dots in the I_{sp}-N_c plots), there was no systematic variation of the amplitude of current spike with the number of cycles and the slope values are spreading randomly in the range from -0.02 A/cycle to +0.02 A/cycle.

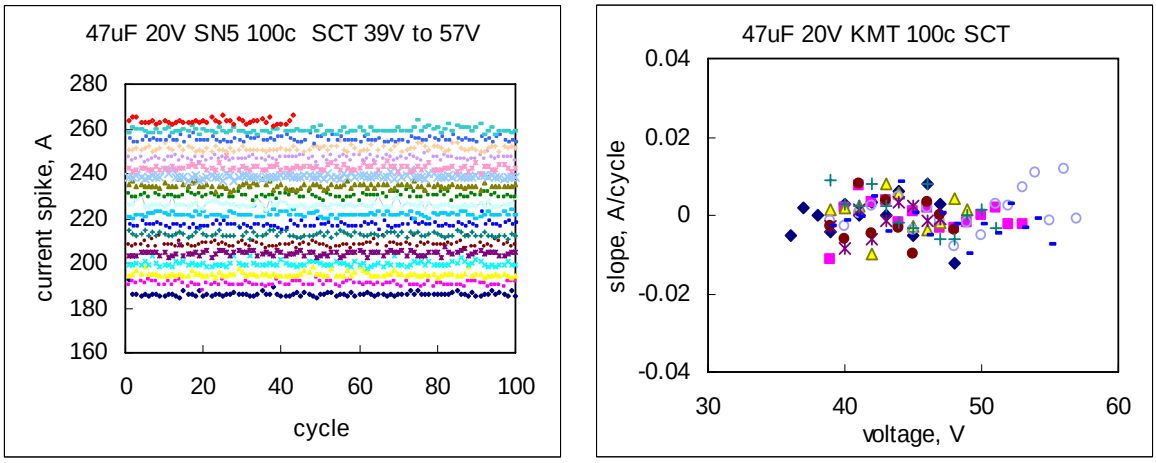

a) b)

Figure VII.2. Variations of current spike amplitudes for a 47 µF/20 V capacitor with the number of cycles during 3SCT starting from 39 V in 1 V increments (a), and dependence of the slope on stress voltage during 100-cycle testing of 9 samples. Note that SN5, Figure (a), failed cycle 43 at 57 V.

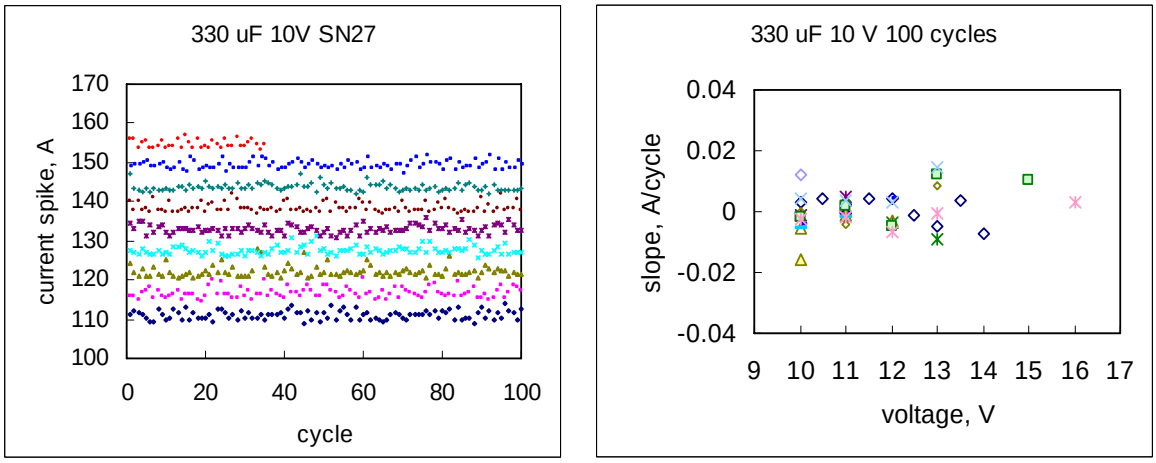

a) b)

Figure VII.3. Variations of current spike amplitudes for a 330 µF/10 V capacitor with the number of cycles during 3SCT starting from 10 V in 0.5 V increments (a), and dependence of the slope on stress voltage during 100-cycle testing for 14 samples. Note that SN27, Figure (a), failed cycle 35 at 14 V. Each dot on the chart (a) corresponds to one surge current cycle.

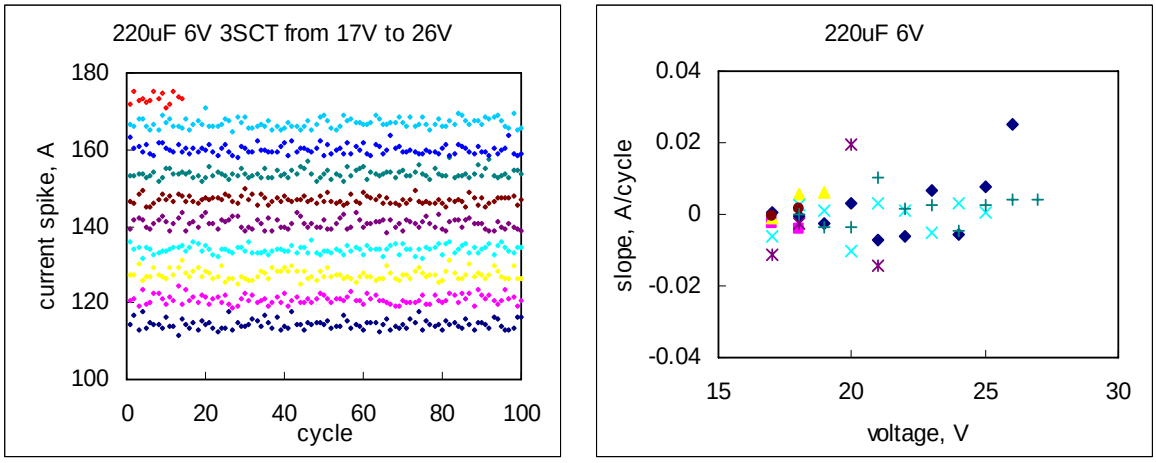

a) b)

Figure VII.4. Variations of current spike amplitudes for a 220 µF/6 V capacitor with the number of cycles during 3SCT starting from 17 V in 1 V increments (a), and dependence of the slope on stress voltage during 100-cycle testing for 7 samples. Note that the sample in Figure (a) failed cycle 15 at 25 V.

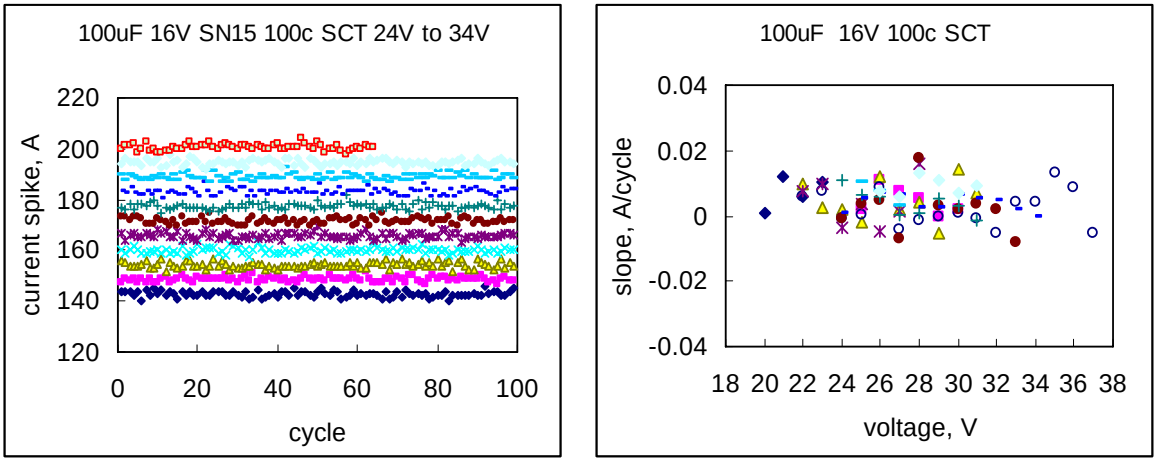

a) b)

Figure VII.5. Variations of current spike amplitudes for a 100 µF/16 V capacitor with the number of cycles during 3SCT starting from 24 V in 1 V increments (a), and dependence of the slope on stress voltage during 100-cycle testing for 10 samples. Note that the sample in Figure (a) failed cycle 65 at 34 V.

VII.2. Breakdown voltages and number of cycles to failure during 3SCT.

Nine samples of 33 µF/35 V KEMET capacitors, which passed SCT screening for 10 cycles at 50 V, were tested at 70 V for up to 100 cycles. The voltage of this test condition was chosen to be close to the mean breakdown voltage for these parts (72 V), to precipitate a large proportion of

failures. Results of the test are shown in Table VII.3 and indicate that at these conditions the parts can fail at any number of cycles in the range from 1 to more than 100.

Table VII.3. Cycles to failure for 33 μF/35 V capacitors tested at 70 V for up to 100 SCT cycles.

	Cycle to Failure
SN1	42
SN2	1
SN3	68
SN4	13
SN5	11
SN6	30
SN7	>100
SN8	14
SN9	11

A group of 18 samples of 22 μF/35V capacitors was subjected to 10-cycle-per-step, 2 V increments, 3SCT starting from the rated voltage. The breakdown voltages and the number of cycles to failure at the last step are shown in Table VII.4. Five out of 18 parts (28%) failed at the first cycle and the rest apparently failed randomly between the first and the last cycle. No correlation between the number of cycles to failure and the breakdown voltage was observed.

Table VII.4. Failure conditions of 22 μF/35 V capacitors during 10-cycle-per-step 3SCT from 35 V in 2 V increments.

	V_{BR}_3SCT, V	Cycle
SN1	63	1
SN2	69	3
SN3	69	9
SN4	59	6
SN5	67	4
SN6	69	3
SN7	65	2
SN8	69	4
SN9	57	1
SN10	73	6
SN11	59	1
SN12	47	5
SN13	67	9
SN14	45	3
SN15	75	8
SN16	81	1
SN17	67	10
SN18	65	1

Results of 10- and 100-cycle-per-step 3SCT at $\Delta V = 1$ V for 220 μF/6 V capacitors are shown in Table VII.5. During this test ~53 % of parts failed at first cycle during 10-cycle test, whereas only 20 % failed at first cycle after passing 100 cycles at a voltage only 1 V lower than the breakdown voltage. Seven out of 10 parts failed at N_f more than 10. The number of cycles to failure in the rest of the group apparently varied randomly from 1 to 99 cycles, also without correlation to V_{BR}_3SCT.

Table VII.5. Failure conditions of 220 μF/6 V capacitors during 10- and 100-cycle-per-step 3SCT in 1 V increments.

	10 cycles in 1V incr.		100 cycles in 1V incr.	
	V_{BR}_3SCT	cycle	V_{BR}_3SCT	cycle
SN1	19	3	19	31
SN2	18	6	20	14
SN3	20	1	21	1
SN4	22	4	23	99
SN5	19	1	26	5
SN6	19	2	21	27
SN7	20	1	26	1
SN8	21	1	27	16
SN9	26	6	24	72
SN10	20	1	20	92
SN11	17	1		
SN12	26	1		
SN13	22	1		
SN14	22	5		
SN15	16	2		
SN16	20	3		
SN17	21	1		

Three groups of 47 μF/20 V KEMET capacitors were tested at different 3SCT conditions. The first group had 10 cycles per step and voltage increment $\Delta V = 2$ V; the second was tested at 100 cycles per step and $\Delta V = 1$ V; and the third also had 100 cycles-per-step, but 2 V increments. Results of testing are displayed in Table VII.6. The first and the third groups had relatively large proportions of the first cycle failures (77% and 50%), whereas only 33% of parts failed during the first cycle in the second group. This indicates that the proportion of first cycle failures increases with the voltage increment. The majority of the parts in the second group (55%) had N_f exceeding 10.

Table VII.6. Results of 3SCT at 10 and 100 cycles per step for 47 μF/20V capacitors.

	10 cycles in 2V incr.		100 cycles in 1V incr.		100 cycles in 2V incr.	
	V_{BR}_3SCT	cycle	V_{BR}_3SCT	cycle	V_{BR}_3SCT	cycle
SN1	52	1	47	51	32	10
SN2	60	1	35	1	44	1
SN3	48	1	53	77	38	1
SN4	50	2	50	5	46	4
SN5	54	9	57	43	42	1
SN6	52	1	48	1	38	2
SN7	50	1	48	25		
SN8	38	4	52	82		
SN9	52	1	56	1		
SN10	50	1				
SN11	24	1				
SN12	26	1				
SN13	52	1				

Table VII.7 shows failure conditions for two groups of 330 μF/10 V capacitors tested at 10- and 100-cycle-per-step 3SCT in 1 V increments. Most parts failed after the first cycle during 10-cycle

test, but only 33% of parts had $N_f = 1$ during 100-cycle test. Seven out of 18 parts failed at $N_f > 10$ without correlation with the breakdown voltage.

Table VII.7. Results of 3SCT at 10 and 100 cycles per step for 330 μF/10 V capacitors.

	10 cycles in 1V incr.		100 cycles in 1V incr.	
	V_{BR}_3SCT	cycle	V_{BR}_3SCT	cycle
SN1	11	1	12	66
SN2	11	1	12	9
SN3	10	2	14	6
SN4	11	1	12	10
SN5	10	1	13	11
SN6	9	1	12	1
SN7	11	1	10	3
SN8	9	1	13	1
SN9	11	1	12	1
SN10	10	1	11	1
SN11	12	2	14	35
SN12			12	45
SN13			12	2
SN14			13	58
SN15			15	1
SN16			10	33
SN17			13	37
SN18			17	1

Results of 10- and 100-cycle 3SCT for two groups of 100 μF/16 V capacitors tested in 1 V increments are shown in Table VII.8. A large proportion of these parts (30%) failed 100-cycle 3SCT after more than 10 cycles. Similar to results obtained for other part types, the majority (75%) of 100 μF/16 V capacitors failed first cycle when subjected to the 10-cycle-per-step testing, whereas only 30% failed first cycle during the 100-cycle testing. This can be explained assuming that the parts failing 100-cycle test after more than 10 cycles would fail most likely first cycle at the next voltage step during 10-cycle 3SCT.

Table VII.8. Results of 3SCT at 100 cycles per step for 100 μF/16 V capacitors.

	10 cycles in 1V incr.		100 cycles in 1V incr.	
	V_{BR}_3SCT	cycle	V_{BR}_3SCT	cycle
SN1	35	1	24	2
SN2	29	10	31	1
SN3	32	1	31	43
SN4	29	1	38	1
SN5	28	1	29	1
SN6	25	1	33	62
SN7	31	1	32	3
SN8	32	1	34	65
SN9	27	3	28	3
SN10	29	1	32	2
SN11	25	1		
SN12	38	7		

To analyze the correlation between the breakdown voltages and the number of cycles-to-failure, N_f values obtained during 1 V increment, 100-cycle 3SCT were plotted against the normalized

breakdown voltage, VBR_3SCT/VR, in Figure VII.6. The data clearly indicate an absence of correlation between N_f and VBR. Out of 55 samples tested at 100-cycle-per-step, 1 V increment 3SCT, 53% failed after 10 cycles.

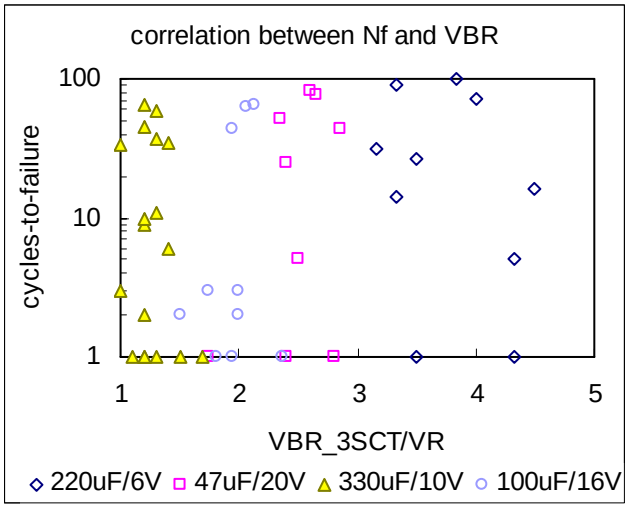

Figure VII.6. Correlation between the number of cycle-to-failure and breakdown voltage rated to VR during 100-cycle 3SCT in 1 V increment for 220 µF/6 V, 47 µF/20 V, 330 µF/10 V, and 100 µF/16 V capacitors.

The data for 330 µF/10 V parts show that even at the rated voltage, failures after more that 10 cycles do happen. For other part types failures at V_{test} = VR were not observed due to much higher characteristic breakdown voltages (see Table III.2.) and respectively much lower probability of failures at VR. However, the absence of N_f -VBR_3SCT correlation allows the assumption that a relatively large proportion of parts failing at VR might fail at N_f exceeding 10 cycles. This means that post-screening failures are possible, and the lower the characteristic breakdown voltage, the greater the probability of these failures.

Statistical data for breakdown voltages measured during 3SCT at 1-, 10-, and 100-cycle-per-step for different part types are summarized in Table VII.9 and displayed in Figure VII.7. It was expected that increased numbers of cycles per step, N_c, would decrease the breakdown voltage. However, the data do not indicate any trend in variation of VBR_3SCT with N_c. This is likely due to the relatively large spread of the breakdown voltages and the small number of tested samples. For 47 µF/20 V and 22 µF/35 V parts, the breakdown voltages appear to increase with the number of cycles. However, statistical analysis showed that at the confidence level of 95%, an increase of VBR_3SCT can be confirmed for 47 µF/20 V parts when comparing 1-cycle and 100-cycle tests only.

Table VII.9. Effect of number of cycles during 3SCT on breakdown voltages.

part	1 cycle			10 cycles			100 cycles		
	QTY	Average	STD	QTY	Average	STD	QTY	Average	STD
330 μF 10 V	26	10.8	1.68	11	9.64	0.99	22	11.16	2.34
220 μF 6 V	36	19.85	4.52	28	19.91	2.78	25	17.35	5.05
47 μF 20 V	65	40.15	8.87	14	43.84	10.13	9	48.77	6.82
100 μF 16 V	43	27.8	6.24	19	26.13	5.6	16	26.75	6.13
22 μF 35 V	33	57.94	11.12	18	62.99	9.29			

It is conceivable that some hardening of the parts occurs during multiple surge current cycling, causing an increase of breakdown voltages. Results obtained by Franklin [4] also indicate that surge testing at lower stress levels can clear some of the faults and improve quality of the parts. Our data show that there is no significant difference in VBR_3SCT between results obtained at different numbers of cycles per step. It is possible that both trends, clearing of some faults and damage accumulation, resulting in decrease of VBR_3SCT, coexist resulting in a complex N_f(VBR) relationship. Additional analysis is necessary to evaluate the effect of N_c on the surge current breakdown voltages more accurately.

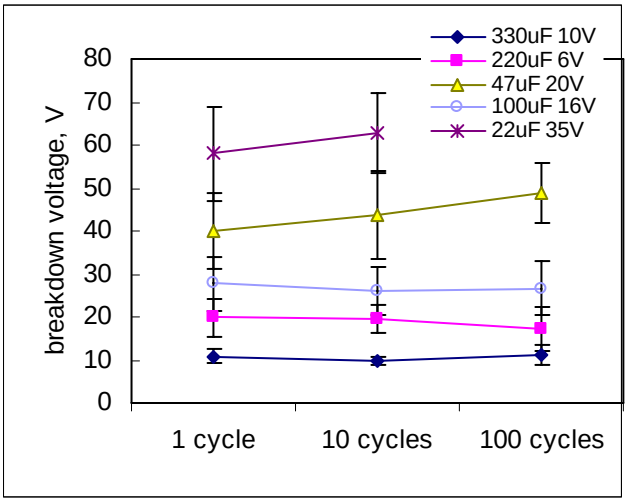

Figure VII.7. Average breakdown voltages measured during 3SCT at different numbers of cycles per step.

VIII. Discussion.

As 100-cycle 3SCT experiments showed, a large proportion of parts in different lots can withstand more than 1,000 cycles (up to 20 100-cycle steps in 1V increment) at voltages gradually increasing from the rated one. Considering possible accelerating factors of the increased stress voltages, it is reasonable to assume that at rated voltages these parts would be able to withstand more than hundreds of thousands of cycles. This means that tantalum capacitors can sustain a practically unlimited number of surge current cycles at low enough voltages. Given that most lots had characteristic breakdown voltages much greater than the rated one, it is possible that the majority of parts in such lots would never fail at the rated voltage. This is consistent with results reported by many authors and implies the existence of a certain threshold voltage, V_{th}, below which surge current failures do not occur.

All parts failing 100-cycle 3SCT at a certain breakdown voltage could withstand more than 100 cycles at a voltage that only 1 V less than the breakdown one. This indicates that there is a relatively narrow range of voltages above V_{th}, at which parts are failing and this range is specific for each capacitor.

A large proportion of parts fail after more than 10 surge cycles, and the number of cycles to failure does not correlate with the breakdown voltage. This casts some doubt upon the common perception that if a part does not fail during the first several surge current cycles, it will never fail under an increased number of cycles. This also impedes the credibility of the existing screening procedure and indicates the possibility of post-screening failures. The probability of failures at $N_f > 10$ is likely to decrease substantially as the test voltage decreases, but for some lots it might be unacceptably high. Considering dramatic consequences of failures of tantalum capacitors in high-reliability applications, this probability cannot be neglected without assessment.

A model of surge current failures has been developed to explain experimental data, assess the probability of surge current failures, and evaluate the effectiveness of SCT screening.

VIII.1. Modeling of the number of cycles to failure.

The suggested model is based on the following assumptions:

1. For each part there is a minimal, critical voltage, V_{cr}, at which the part fails after the first surge current cycle.
2. There is a certain threshold voltage, V_{th}, below which the part would never fail.
3. At voltages between V_{th} and V_{cr} the part might fail at any number of cycles, N_f, and this number is increasing at voltages closer to V_{th}.
4. Failures at $N_f > 1$ are due to accumulated damage caused by the previous cycles and the failure condition is determined by Miner's rule:
   $$N_f \times D = 1 \ , \qquad (1)$$
   where D is damage produced by one surge current cycle.
5. The value of damage depends on the difference between the stress voltage and V_{th} according to a power law:

$$D = A(V - V_{th})^n \ , \qquad (2)$$

where A and n are constants.

Combining Eq. (1) and (2) N_f can be expressed as follows:

$$N_f = \frac{1}{A \times (V - V_{th})^n} \ , \qquad (3)$$

Assuming that the value of $(V-V_{th})$ represents the damage-creating stress in the part, Eq. (3) can be considered similar to the empiric Coffin-Manson model for failures in components and materials induced by mechanical stress cycling. The applicability of this model can be justified assuming that the surge current failures are due to mechanical shocks developed in the part during surge current events. For the Coffin-Manson model, parameter n is typically close to 2, so by adopting this model it can be assumed also that in Eq.(3) n = 2.

Considering that at $V = V_{cr}$, $N_f = 1$, constant A can be determined from Eq.(3):

$$A = \frac{1}{(V_{cr} - V_{th})^n} \ , \qquad (4)$$

In this case, the number of cycles to failure can be expressed as follows:

$$N_f = \left(\frac{V_{cr} - V_{th}}{V - V_{th}} \right)^n \ , \qquad (5)$$

Note that V_{th} is less than V_{cr}. This allows expressing the threshold voltage as a portion, α, of the critical voltage:

$$V_{th} = \alpha \times V_{cr} \ , \qquad (6)$$

where $\alpha < 1$.

Using parameter α, Eq.(5) can be simplified and written in the following form:

$$N_f = \left(\frac{1 - \alpha}{V / V_{cr} - \alpha} \right)^n \ , \qquad (7)$$

Obviously, at $V/V_{cr} \leq \alpha$ no failures occur and at $V \geq V_{cr}$ surge current failures would occur during the first test cycle. Considering a relatively narrow range of voltages, where surge current failures were observed, parameter α is likely to vary in a range from 0.8 to 1.

Variations of N_f with the test voltage at different values of α are shown in Figure VIII.1 and indicate that even relatively minor variations in α can cause significant changes in N_f and, more importantly, change the minimal voltage above which surge current failures might occur. Parameter α, together with V_{cr}, indicates the range of voltages, in which the part can fail after a number of cycles. Additional analysis showed that some variations in the exponent n in Eq. (7) do not change results of SCT simulation dramatically. However, parameter α determines "never fail" and the first-cycle-failure conditions, and is the most important parameter of the model.

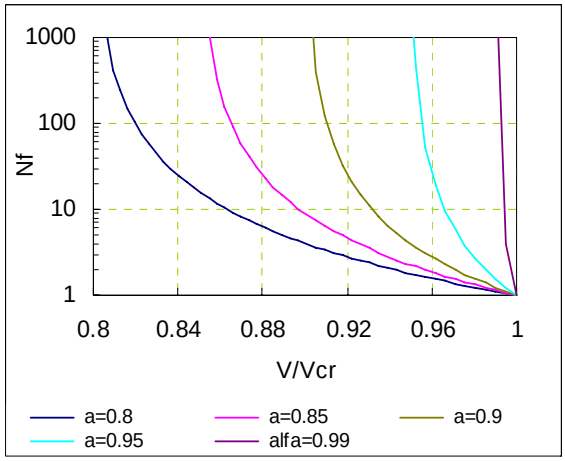

Figure VIII.1. Variations of the number of cycles to failure with voltage at different values of the model parameter α calculated per Eq.(6).

The values of V_{cr} can be obtained experimentally during one-cycle 3SCT. Considering that for a given lot, the distribution of V_{cr} is described using a Weibull function with a characteristic breakdown voltage η and shape parameter β, the value of V_{cr} can be expressed via the probability, p, of the part to have $V_{BR} \le V_{cr}$:

$$V_{cr} = \eta \times \left[-\ln(1-p)\right]^{1/\beta}, \qquad (8)$$

This allows for numerical modeling (Monte Carlo simulation) of the probability of a part to fail after a certain number of cycles. By setting random values of the probability p, $0 < p < 1$, a group of samples having individual values of V_{cr} can be generated using Eq.(8). Then for each sample a number of cycles to failure can be calculated using Eq.(7) for a range of stress voltages $\alpha V_{cr} < V < V_{cr}$. For voltages outside this range, we assume $N_f = 1$ at $V \ge V_{cr}$, and $N_f = \infty$ at $V < \alpha V_{cr}$. A graphical presentation of this simulation methodology is shown in Figure VIII.2.

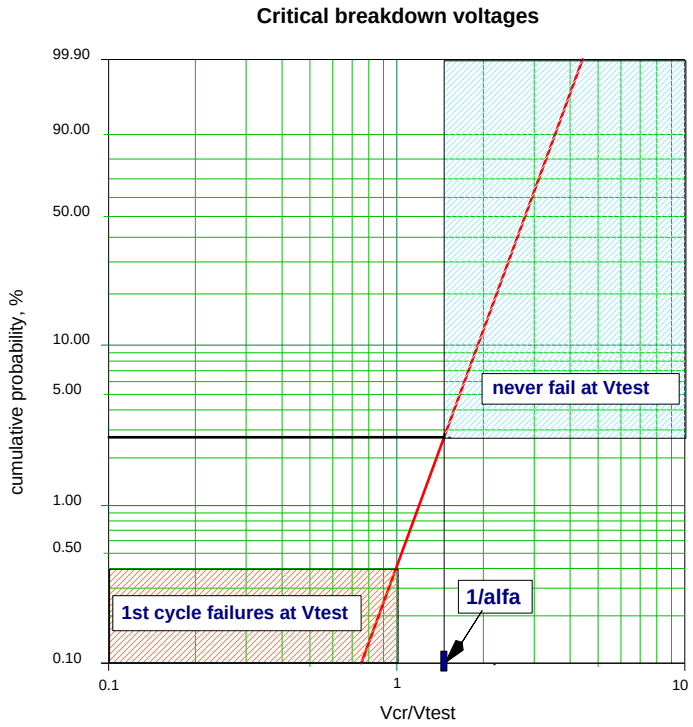

Figure VIII.2. An explanatory Weibull distribution of the critical breakdown voltages rated to the test voltage. The area shown by red hatching indicates the "first cycle" failures and the blue-hatched area shows "no failure" conditions. The area where the part can fail at any number of cycles is in between.

VIII.2. 3SCT simulation.

Using a concept described in the previous section, a Visual Basic program to simulate 3SCT has been developed. The damage after each step prior to failure was calculated as a ratio of the number of cycles at each step, N_c, to the number of cycles to failure, N_f, $D_i = N_c/N_{f,i}$. The accumulated damage was a sum of the step damages:

$$D = \sum D_i = \sum_i \frac{N_c}{N_{f,i}} \quad , \qquad (9)$$

where

$$N_{f,i} = (1 - D) \times N_f \quad , \qquad (10)$$

As soon as the condition $N_{f,i} < N_c$ is satisfied, the virtual testing stopped and the program recorded the breakdown voltage, VBR_3SCT, equal to the last voltage step, and the number of cycles to failure at this step, N_f.

Experimental data (see Tables VII.5 to VII.8) suggest that a proportion of the parts failing the first cycle substantially decreases from 55% to 85% at 10 cycle-per-step to 20% to 33% at 100 cycle-per-step. To evaluate the model and estimate its parameters, 3SCT was simulated at $N_c = 10$ and

N_c = 100 by generating 100 virtual samples at η/VR = 2, β = 5, and voltage increment, ΔV/VR = 0.1. Figure VIII.3 shows variation of the proportion of the first-cycle failures with the number of cycles calculated at different parameters α. Comparing these results with experimental data indicates a reasonable agreement at α in the range from 0.9 to 0.95.

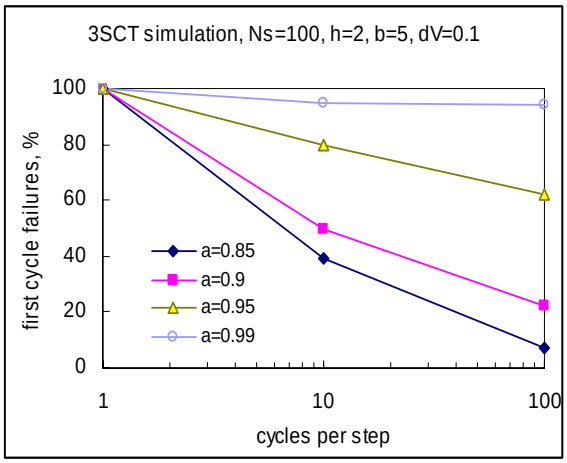

Figure VIII.3. Variation of the proportion of parts failing the first cycle during 3SCT with the number of cycles per step calculated for parts having a Weibull distribution of V_{cr} with parameters η/VR = 2 and β = 5.

Distributions of the breakdown voltages calculated during 3SCT simulations at different N_c are shown in the Weibull plot in Figure VIII.4. The results failed to indicate any trend in the variation of breakdown voltages with the number of cycles, which is also consistent with experimental data.

Another experimental observation is a substantial increase of the proportion of first-cycle failures, N1, during 3SCT as the voltage increment increases. Figure VIII.5 shows variations of N1 and the probability of parts to fail at the number of cycles more than 10, N11, with α at ΔV/VR = 0.05 and 0.1. The results indicate that at α = 0.9, N1 increases from 7% at ΔV/VR = 0.05 to 22% at ΔV/VR = 0.1 and the proportion of parts failing after 10 cycles decreases from 70% at ΔV/VR = 0.05 to 24% at ΔV/VR = 0.1. This is also in reasonable agreement with the experimental data.

Figure VIII.6 shows correlation between the 100-cycle 3SCT breakdown voltages and N_f calculated for 20 samples from the lot having β = 5 and η/VR = 2. A comparison with Figure VII.6 shows that for α in the range from 0.85 to 0.95 the results are comparable, whereas calculations at α = 0.99 resulted in a much higher proportion of the first-cycle failures.

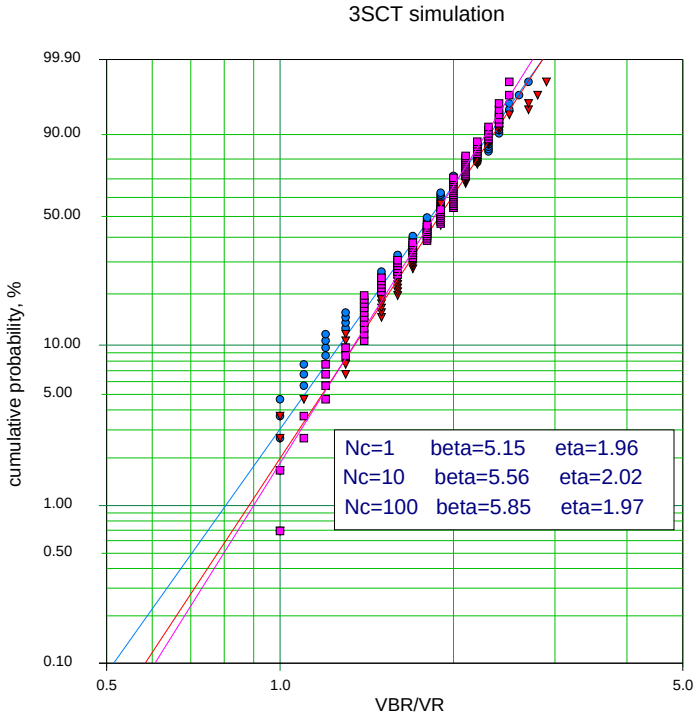

Figure VIII.4. Weibull distributions of simulated 3SCT breakdown voltages at different numbers of cycles per step.

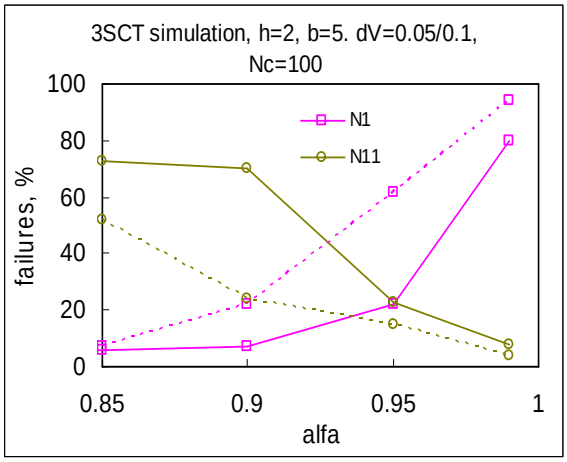

Figure VIII.5. First-cycle failures (N1) and failures after 10 surge cycles (N11) during 3SCT simulations at $0.85 < \alpha < 0.99$ and voltage increments of 0.05 (solid lines) and 0.1 (dashed lines).

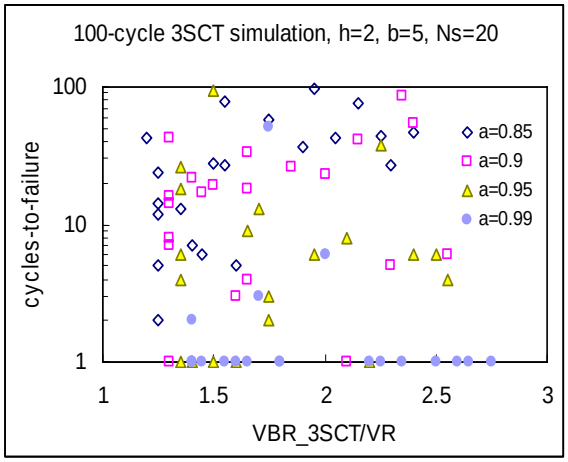

Figure VIII.6. Correlation between the simulated 3SCT breakdown voltages and number of cycles to failure.

VIII.3. Screening simulation.

Using Monte Carlo simulations, proportions of parts having first-cycle failures, N_f1, parts failing between the first and tenth cycle, N_f1_10, parts failing after 10 cycles, N_f11, and "never fail" parts, N_g, were calculated for different η/VR and β values. Obviously, $N_f1 + N_f1\_10$ is the proportion of screening failures and N_f11 is the proportion of post-screening failures. The purpose of separating N_f1 and N_f1_10 is to estimate the proportion of first-cycle failures compared to the total number of screening failures, which is often used as an argument for the effectiveness of the screening. This simulation was carried out by generating 1,000,000 virtual samples having Weibull distribution of V_{cr} with $1 < \eta/VR < 4$ and $\beta = 5$ and 10. Results of these calculations at the model parameter $\alpha = 0.9$ and $\alpha = 0.99$ are shown in Figure VIII.7.

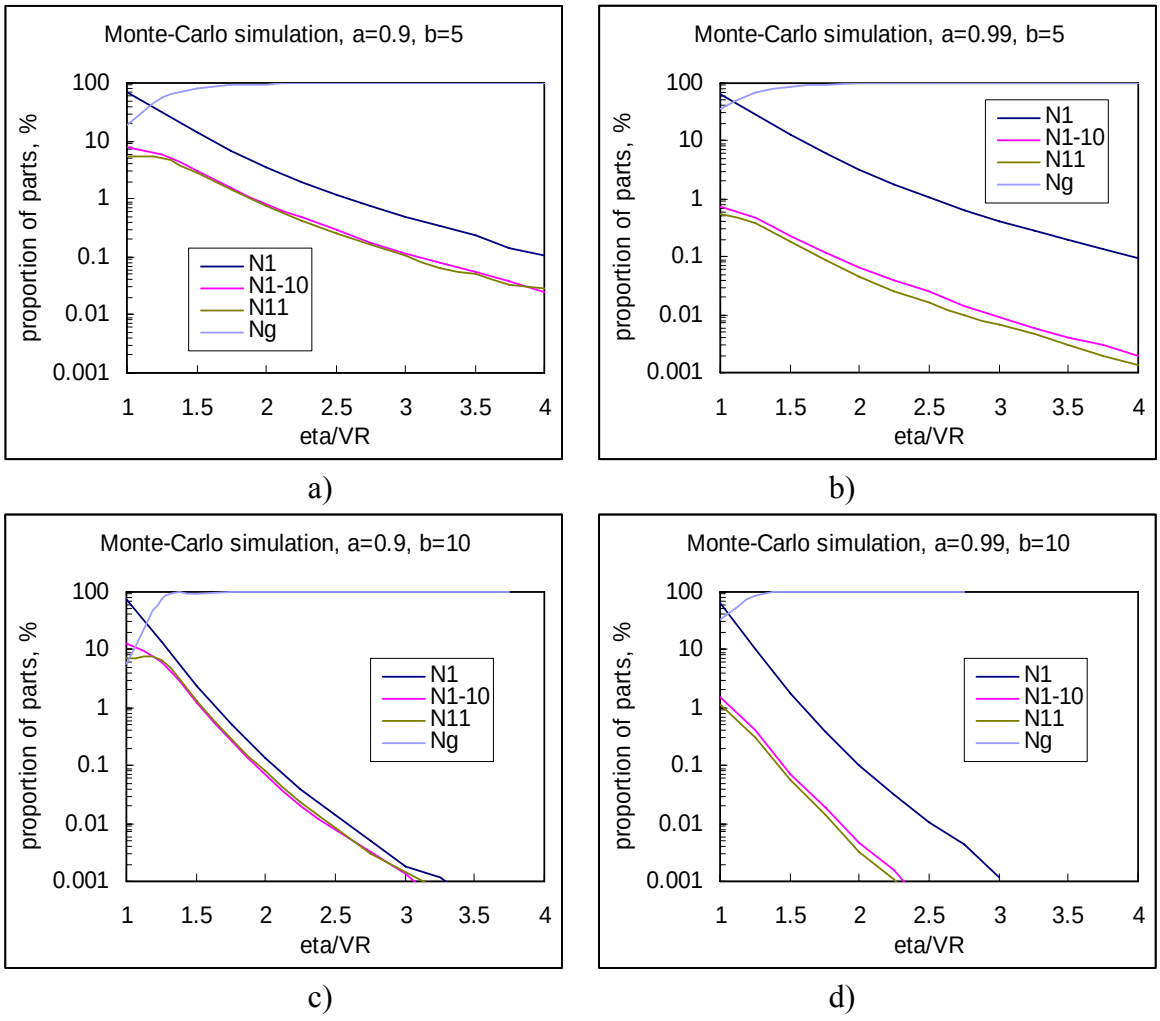

Figure VIII.7. Calculated proportion of parts failing at V = VR after the first cycle (N1), from the first to tenth cycles (N1-10), and after the tenth cycle (N11) at different parameters of the model Eq. (6, 7). Ng indicates a proportion of good, "never failed" parts. The data were calculated for $\beta = 5$ (a, b); $\beta = 10$ (c, d); and $\alpha = 0.9$ (a, c), $\alpha = 0.99$ (b, d).

Analysis shows a sharp, near-exponential decrease of the probability of surge current failures with η exceeding 1.5. A similar effect has an increase of the shape parameter: at $\eta/VR = 2$ and $\alpha = 0.9$, a proportion of parts failing SCT decreases from 1.9% to 0.01% as β increases from 4 to 14. At $\alpha = 0.99$ this decrease is even more substantial, from 0.16% at $\beta = 4$ to 6.1E-4% at $\beta = 14$.

For typical cases of lots having $\eta/VR = 2.5$ and $\beta = 5$ and 10, the proportion of screening (10 cycles at VR) failures and post-screening failures at the rated voltage is shown in Figure VIII.8. The first-cycle failures at VR are also shown and indicate that these failures comprise the majority (from 67% to 94%) of all screening failures, which is typically observed during SCT screening. The proportion of post-screening failures is from 3 to 6 times to 66 to 550 times less than the proportion of screening failures, for $\alpha = 0.9$ and $\alpha = 0.99$ respectively. Considering a relatively low probability of surge current failures during regular testing at rated voltages, to reveal the post-screening failures, a large quantity of samples, similar to the one used for simulations, should have been tested by applying hundreds and thousands of surge current cycles. A generally low probability of post-screening failures could explain the common perception that if a part does not fail during the first few cycles, it never fails at a greater number of cycles.

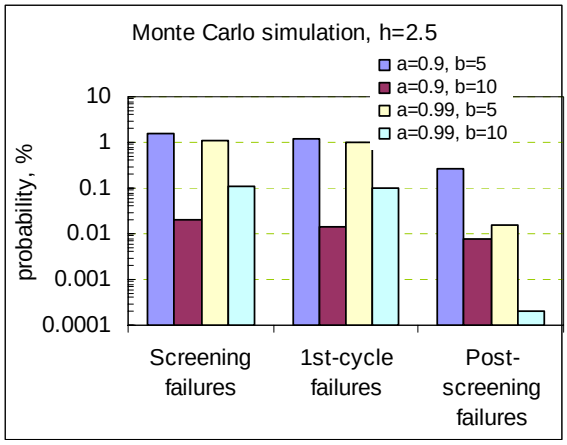

Figure VIII.8. Simulation of screening and post-screening failures.

Figure VIII.9 shows variations of the probability of post-screening failures with parameters of Weibull distributions at α in the range from 0.85 to 0.95. These calculations imitate a regular, 10-cycle screening at the rated voltage. At relatively small shape factors, $\beta < 5$, and characteristic breakdown voltages, $\eta/VR < 2$, the probability of post-screening failures exceeds 0.2%, which is not acceptable for high-reliability applications. For a typical case with $\eta/VR = 2$ and $\beta = 8$, the model predicts that from 0.07% to 0.5% of parts might fail if surge current events at the rated voltage happen after screening. Obviously, the probability of failing first cycle after screening is much lower, but in many cases is not negligible.

To reduce the probability of failures during applications, surge current screening should be performed at voltages exceeding the rated ones. Analysis of the model shows that by increasing screening voltage to $V_{scr} = VR/\alpha$, the majority of post-screening failures can be eliminated. Considering that the most probable range of α is from 0.85 to 0.95, screening should be performed

at voltages 1.1VR to 1.15VR. It should be noted that AVX is routinely performing SCT screening at 1.1VR during manufacturing of their products [12]. This indicates that this test condition is quite realistic, and the requirement for tantalum capacitors to sustain surge current testing at voltages exceeding VR should be included in the relevant specifications for parts used in military and space applications.

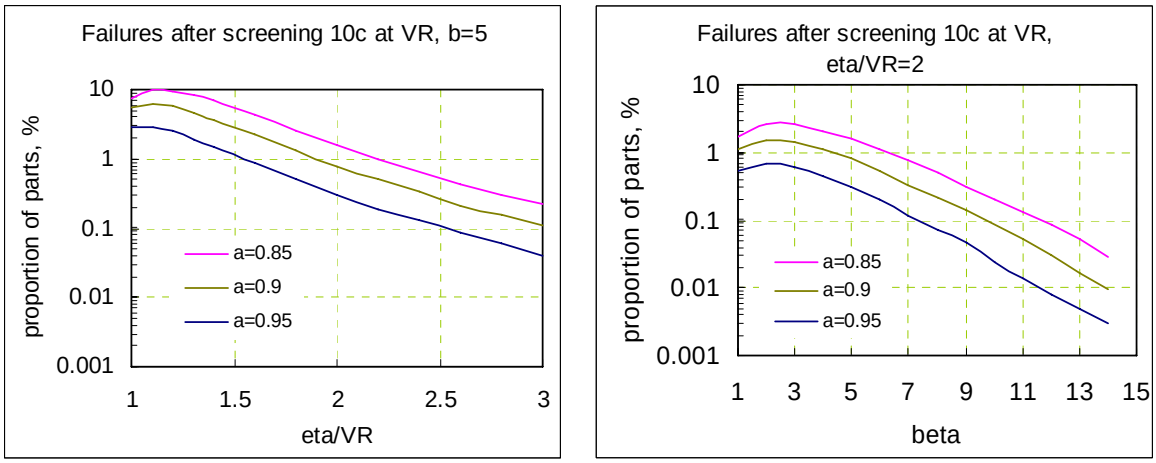

a) b)

Figure VIII.9. Probability of post-screening failures at different parameters of Weibull distributions and α. Screening simulation: 10 cycles at the rated voltage.

An increase in V_{scr} during SCT increases the proportion of parts failing screening by several times (see Figure VIII.10). Calculations show that for cases of lots having Weibull distributions of V_{cr} with η/VR = 2, β = 5 and β = 10, an increase of the proportion of failures varies from ~2X to ~5X as V_{scr} increases from VR to 1.15VR. However, the losses caused by higher fallout rates during screening are compensated by a substantial reduction of the probability of post-screening failures.

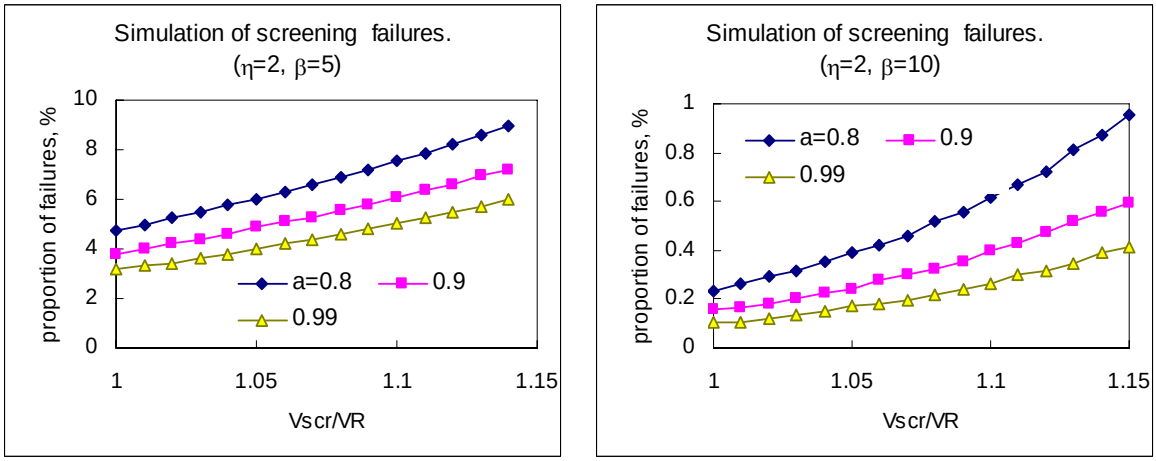

a) b)

Figure VIII.10. The probability of failure during screening vs. screening voltage at different parameters of the model (α = 0.8, 0.9, and 0.99) for parts having Weibull distributions of Vcr with η/VR = 2, β = 5 (a) and β = 10 (b).

Figure VIII.11 shows variation of the proportion of post-screening failures at different screening voltages for the same conditions as in Figure VIII.10. In all cases a substantial decrease in the probability of failures occurs at V_{scr} ~15% greater than the rated voltage. For this reason SCT screening at 1.15VR can be recommended to eliminate most of the post-screening failures.

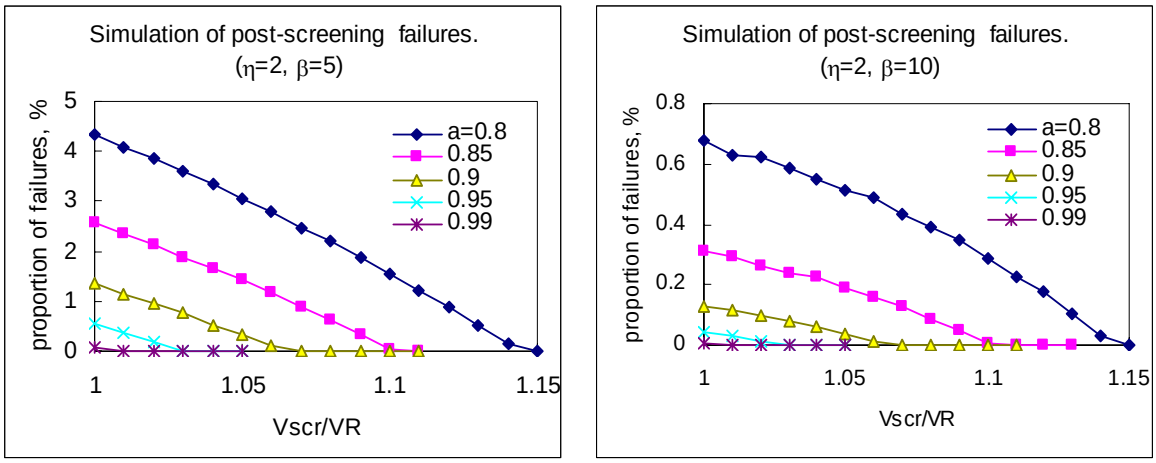

a) b)

Figure VIII.11. The probability of post-screening failures vs. screening voltage at the same parameters of the model as shown in Figure VIII.10.

Although SCT screening of tantalum capacitors is performed at rated voltages, it is strongly recommended that the parts are used in low-impedance applications at 50% derating. For parts with different parameters of the distribution of breakdown voltages, Figure VIII.12 shows the probability of failures during SCT at VR and 0.5VR.

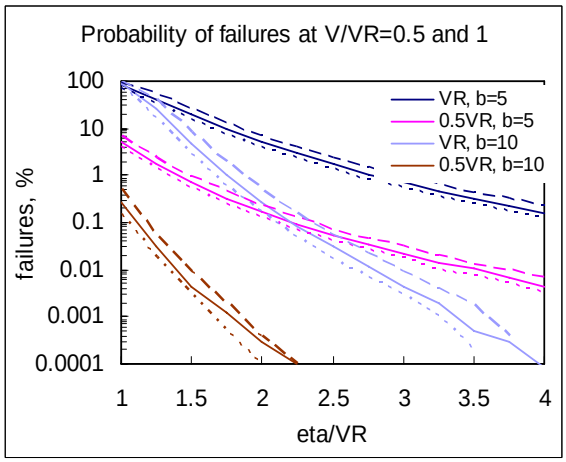

Figure VIII.12. Calculated probabilities of failure during SCT at VR and 0.5VR for parts having Weibull distributions of V_{cr} with $\beta = 5$ and 10 and η/VR varying from 1 to 4. Solid and dashed lines are results of calculations at $\alpha = 0.85$, 0.9, and 0.95.

The results show that unscreened parts might have a relatively high probability of failures even at 50% derating if they have breakdown voltages described by distributions with relatively low values of shape factors, $\beta < 5$, and low characteristic breakdown voltages, $\eta/VR < 2$. Obviously, these failures can be eliminated by SCT screening at the rated voltage. However, in many cases this derating is not justified and might impede the application of high-performance (large C, low ESR, low volume) capacitors in high-reliability systems. Besides, there is a permanently increasing need in use of large-capacitance parts at higher voltages, and taking advantage of increased reliability of contemporary tantalum capacitors, many electronic designers are using parts derated to 0.8VR only.

Recent studies of solid electrolytic capacitors with polymer cathodes and niobium oxide capacitors showed that these parts might be more robust in surge current conditions, do not fail catastrophically due to exothermic reactions, and their recommended derating is much less severe compared to the manganese cathode tantalum capacitors [1, 20]. Additional study of new technology capacitors is necessary to evaluate their capability to withstand multiple surge current cycles and assess the effectiveness of SCT screening. The developed methodology for evaluation of the surge current breakdown voltages and numbers of cycles to failure might be useful for this analysis.

IX. Conclusion.

1. Surge current breakdown voltages were measured on 10 different types of solid tantalum capacitors using a step stress surge current testing technique allowing automatic measurements of the current spike amplitudes, I_{sp}, and effective resistance of the circuit, R_{eff}. Measurements of I_{sp} and R_{eff} verify that adequate, low-resistive contacts to the DUT are used, characterize the test setup, and are important in assuring reproducible results of the test.
2. Amplitudes of current spikes during charge and discharge testing were similar. However, breakdown voltages during step discharge current testing were significantly (>20%) higher than during 3SCT. This indicated that current spikes alone, even when they were limited by ESR only and exceeded hundreds of amperes, did not result in failures. The presence of voltage after the spike was completed is necessary to cause surge current breakdown of the part.
3. Experiments showed that the shape of pulses at the gate of the FET switch and the length of wires connecting the DUT to the SCT circuit might substantially change the amplitude of current spikes. The current spike amplitude was decreased by approximately 1.7 times when the length of wires was increased from 4" to 24". However, the increased length of the wires resulted in a much less significant variation (~5%) of the surge current breakdown voltages, likely because the amount of energy dissipated in the circuit did not depend on the inductance of wires.
4. Based on results of 3SCT for three part types, temperature dependence of surge current breakdown voltages, at least in the range from room to 85 ^{o}C, follows Arrhenius law. However, the activation energy was low and varied from 0.007 eV to 0.015 eV only. In one part type, VBR_3SCT decreased at low temperatures ~5% at -55 ^{o}C and ~12% at -196 ^{o}C compared to room temperature, likely due to an increased level of mechanical stresses.
5. Results of 3SCT for the 10 part types showed that the characteristic breakdown voltages of Weibull distributions exceeded the rated voltages by two times on average. However, the spread of this ratio was large and varied from 1.2 to 3.6, resulting in a situation in which parts with a lower rated voltage had much higher breakdown voltages than parts rated to a higher voltage. This means that generally, the rated voltage was not an indicator of the robustness of the parts in surge current environments. The shape factors for VBR_3SCT distributions averaged 7.9 with a spread from 5.2 to 14.3. For some part types, bimodal Weibull distributions provided a better fit than unimodal distributions thus indicating the presence of low-voltage and high-voltage subgroups in the lot.
6. Measurements of characteristics of the 10 types of capacitors during surge current testing at increasing numbers of cycles (up to 2000 for charge-, and to 7 million for discharge) and stress voltages (up to 2VR in some cases) revealed no evidence of substantial variations of AC or DC characteristics of the parts. This indicates that chip tantalum capacitors are capable of withstanding a practically unlimited number of high current spikes (more than 100 amperes) without any degradation.
7. Five part types with groups of 32 to 50 parts were subjected to accelerated life testing at 125 ^{o}C and V = 1.5VR for up to 250 hours. To simulate screening conditions, half of the samples were stressed prior to the testing by 10 to 30 SCT cycles at 1.5VR. Life testing resulted in a statistically significant number of failures, but no differences in the test results between the

SCT-screened and non-screened groups were observed. Additionally, four part types were tested at room temperature and 2VR for 200 hours, while leakage currents were monitored to record scintillation events (failures). Similar to life testing at 125 ^{o}C, statistical analysis showed no difference in the proportion of failures in groups with and without SCT screening.

8. To evaluate the effect of Weibull grading on surge current breakdown voltages, 3SCT was carried out on parts after life testing. Analysis showed no significant effect of the life testing at 125 ^{o}C; however, room temperature long-term stress of the parts at high voltages increased surge current breakdown voltages by 10% to 20%.
9. Results obtained for the SCT-screened and non-screened parts before and after life testing showed that SCT screening was not a significant factor in life testing. Also, the life test did not degrade surge current breakdown voltages. For this reason, options B and C per MIL-PRF-55365 can be considered as equivalent.
10. Parts that failed life testing had surge current breakdown voltages similar to virgin parts, thus indicating that self-healed scintillation breakdowns likely do not degrade the capability of capacitors to withstand surge current conditions. However, parts that were capable of withstanding hundreds of hours of steady-state testing at 2VR, failed 3SCT at voltages much lower than 2VR. This suggests that the scintillation and surge current breakdowns probably have different mechanisms, and "proofing" of the parts does not guarantee their reliability under surge current conditions.
11. Results of SCT with multiple cycling at different voltages showed no evidence of degradation even at voltages close to the breakdown, and indicated that at relatively low voltages solid tantalum capacitors can withstand a practically unlimited number of cycles. This suggests that there is a certain threshold voltage, V_{th}, below which surge current failures do not occur.
12. All parts failing 100-cycle 3SCT at a certain breakdown voltage could withstand more that 100 cycles at a voltage only 1 V less than the breakdown one. This indicates that there is a relatively narrow range of voltages above V_{th} at which the parts can fail, and this range is specific for each capacitor.
13. The results of 3SCT at 10 and 100 cycles per step and low voltage increments showed that the parts can fail at any number of cycles, N_f, which apparently randomly varies from 1 to 100 without correlation with the breakdown voltage. A relatively large proportion of parts, 53% out of 55 samples tested at 100 cycles per step and 1 V increments, failed after more than 10 cycles.
14. Multiple surge current cycling at rated voltages revealed failures after more than 10 cycles only in one lot, 330 μF/10 V capacitors. For other part types, failures at VR were not observed due to much higher characteristic breakdown voltages and, respectively, a much lower probability of failures. However, the absence of N_f -VBR correlation allows the assumption that a relatively large proportion of parts might fail at N_f exceeding 10 cycles even at the rated voltage. This means that post-screening failures are possible in all lots, and the lower the characteristic breakdown voltage, the higher the probability of these failures.
15. A model of surge current failures allowing calculations of the number of cycles to failure for a given distribution of V_{cr} (a minimum voltage resulting in surge current failure at the first cycle), has been developed. Simulation of 3SCT using Eq.(7) and (8) showed a reasonable agreement with the experimental data at the model parameters α in the range from 0.85 to 0.95

and n = 2. At relatively small shape factors, $\beta < 5$, and characteristic breakdown voltages, $\eta/VR < 2$, the model predicted a rather high probability of post-screening failures exceeding 0.2%, which is not acceptable for high-reliability applications.

16. To reduce the probability of failures during applications, surge current screening should be performed at voltages exceeding the rated ones. Analysis shows that by increasing screening voltage to 1.1*VR to 1.15*VR, the majority of post-screening failures at the rated voltage can be eliminated. The results of experiments presented in this report show that this screening condition does not degrade quality and reliability of chip tantalum capacitors.

X. References.

[1] J. D. Prymak, "Performance issues for polymer cathodes in Al and Ta capacitors," Proceedings of CARTS USA 2001, 2001, pp. 25-34.

[2] M. J. Cozzolino and R. C. Straessle, "Design, characteristics, and failure mechanisms of tantalum capacitors," Proceedings of 8th CARTS'88, San Diego, CA, 1988, pp. 98-110.

[3] K. Lai, E. Chen, P. Blais, P. Lessner, B. Long, A. Mayer, and J. Prymak, "Step Surge Stress Test (SSST) Defines Dielectric Capability," Proceedings of CARTS in Asia, Taiwan, 2007, pp.

[4] R. W. Franklin, "Surge current testing of resin dipped tantalum capacitors," *AVX technical information*, 1985. http://www.avxcorp.com/docs/techinfo/dipptant.pdf.

[5] H. W. Holland, "Effect of high current transients on solid tantalum capacitors," *KEMET Engineering bulletin*, 1996.

[6] D. Mattingly, "Increasing reliability of SMD tantalum capacitors in low impedance applications," *AVX technical information*, 1995. http://www.avxcorp.com/docs/techinfo/tantimp.pdf.

[7] J. Gill, "Surge in solid tantalum capacitors," *AVX Technical information*, 1995. http://www.avxcorp.com/docs/techinfo/surgtant.pdf.

[8] B. S. Mogilevsky, G.;, "Surge Current Failure in Solid Electrolyte Tantalum Capacitors," *IEEE Transactions on Components, Hybrids, and Manufacturing Technology*, vol. 9, pp. 475 - 479, 1986.

[9] P. Fagerholt, "A new view on failure phenomena in solid tantalum capacitors," Proceedings of 16th Capacitors and Resistors Technology Symposium, CARTS'96, 1996, pp. 162-166.

[10] J. D. Prymak, "Derating Differences in Tantalum-MnO2 vs. Tantalum-Polymer vs. Aluminum-Polymer," Proceedings of 23rd Capacitor And Resistor Technology Symposium, 2003, pp. 278-283.

[11] A. Teverovsky, "Effect of compressive stresses on performance and reliability of chip tantalum capacitors," Proceedings of CARTS Europe, Barcelona, Spain, 2007, pp. 175-190.

[12] T. Zednicek and J. Gill, "Voltage derating rules for solid tantalum and niobium capacitors," Proceedings of CARTS EUROPE, 2003, pp. 44-50.

[13] J. D. Moynihan and A. M. Holladay, "Effectiveness of surge current screening of solid tantalum capacitors," Proceedings of CARTS 1983, Phoenix AZ, 1983, pp. 53-60.

[14] A. Teverovsky, "Effect of Inductance and Requirements for Surge Current Testing of Tantalum Capacitors," Proceedings of CARTS'03, the 26th Symposium for Passive Components, Orlando, FL, 2006, pp. 363-384.
[15] E. K. Reed and J. L. Paulsen, "Impact of circuit resistance on the breakdown voltage of tantalum chip capacitors," Proceedings of CARTS, 2001, pp. 150-156.
[16] A. Teverovsky, "Effect of Temperature Cycling and Exposure to Extreme Temperatures on Reliability of Solid Tantalum Capacitors," Proceedings of CARTS'07, the 27th Symposium for Passive Components, Albuquerque, NM, 2007, pp. 279-306.
[17] B. Long, M. Prevallet, and J. D. Prymak, "Reliability Effects with Proofing of Tantalum Capacitors," Proceedings of The 25th Symposium for Passive Components, CARTS'05, Palm Springs, California, 2005, pp. 167-172.
[18] E. K. Reed, "Tantalum chip capacitor reliability in high surge and ripple current applications," Proceedings of 44th. Electronic Components and Technology Conference, 1994, pp. 861-868.
[19] J. Pavelka, J. Sikula, P. Vasina, V. Sedlakova, M. Tacano, and S. Hashiguchi, "Noise and transport characterisation of tantalum capacitors," *Microelectronics Reliability*, vol. 42, pp. 841-847, 2002.
[20] W. Millman and T. Zedníèek, "Niobium Oxide Capacitors Brings High Performance to a Wide Range of Electronic Applications," Proceedings of CARTS Europe, Barcelona, Spain, 2007, pp. 75-87.